Hydrothermal ZnO; Mastering of Lithium content and formation of Palladium Schottky diodes

Tariq Maqsood

Thesis submitted for the degree of Master of Science

Faculty of Mathematics and Natural Sciences
University of Oslo

July 2008

Acknowledgements

How we treasure (and admire) the people who acknowledge us!

– Julie Morgenstern

I would like to start off by thanking my supervisor Prof. Bengt G. Svensson for pointing me in the right direction, and for always being available for the many small questions I had. His laid back and ever so patient nature makes him an excellent mentor. I would also like to send a special thanks to Ramon Schifano for his (*much* needed) help with the electrical data analysis and the e-beam deposition.

There are also other people at MiNa who deserve my gratitude. Dr. Lars Vines and Dr. Jens Christensen for helping me with the SIMS measurements. Klaus Magnus Johansen for showing me around the lab when I was new. Hans Bjørge Normann, Dr. Jan Håvard Bleka and Hallvard Angelskår for helping me with valuable Matlab-programming. Ole Bjørn Karlsen for his help with polishing the samples. Thor Bakke at SINTEF MiNaLab for letting me borrow the Zygo interferometer for this thesis. Thanks to all the post-docs, Ph.D. and master students for making the two years at MiNa fly by.

Last, but by no means least, thanks to my parents Khalid Maqsood and Bilqees Maqsood for their support, and for letting me stay at home free of charge. My

lovely fiancé Onaza Tahir for encouraging me and standing by me through all these years, and during the finishing stages of my thesis, forcing me to take ice cream breaks – which really did help.

Abstract

For many years now ZnO has been an important ingredient in various products manufactured by the industry, though very few of them utilize its semiconducting properties. Recent advances in growth of high quality, single crystalline ZnO have sparked new interest in the material. Topped with the fact that it has a high exciton binding energy and a wide direct band-gap, makes it the perfect candidate for applications like UV light emitting diodes (LED) and lasers.

In this thesis we have annealed hydrothermally (HT) grown ZnO samples at temperatures ranging from 600°C to 1600°C, and examined the effects on the lithium content, the resistivity and the surface topography. Starting with highly resistive samples, we managed to reduce both the Li concentration and the resistivity with four orders of magnitude each to 10^{13}cm^{-3} and $< 1\Omega\text{cm}$, respectively. Our findings showed a correlation between the Li concentration and the resistivity, and also a polarity effect on the surface roughness resulting from, what we believe, is lithium (Li) diffusion.

We then tuned the resistivity and the surface roughness of some HT ZnO samples, before realizing palladium (Pd) Schottky diodes on the $(000\bar{1})$ O-face, resulting in diodes with following properties: current rectification of up to eight orders of magnitude from -2V to 2V, low series resistance of 20Ω, low ideality factor of 1.06, reverse current density of $J(V = -2) = 10^{-7}\text{A/cm}^2$ and an effective donor concentration of mid-10^{16}cm^{-3}. A surface polarity effect on the diode quality was

also observed.

Contents

1 Introduction **13**

I Lithium content and surface topography after annealing **15**

2 Background **16**
2.1 General semiconductor theory 16
2.2 Crystal defects 18

3 Basic review of ZnO **21**
3.1 ZnO crystal 21
3.2 Lithium 22
3.3 Doping of ZnO 23
3.4 ZnO growth methods 27

4 Sample preparation **29**
4.1 Experimental procedure 29

5 Experimental characterization techniques **33**
5.1 Secondary ion mass spectrometry 33
5.2 Four probe point measurement 37
5.3 White light interferometer 37

6 Results **39**
6.1 Lithium concentration measurements 39
6.2 Resistivity measurements 41
6.3 Surface roughness measurements 41

7 Discussion **45**
7.1 Sample topography 45
7.2 Lithium content 46
7.3 Sample resistivity 49

II Palladium Schottky contacts on hydrothermal ZnO **52**

8 Basic theory of Schottky diodes **53**
8.1 Schottky diode theory 53
8.2 Deviations from ideal Schottky diodes 57

9 Experimental procedure and previous work **59**
9.1 Schottky diode deposition procedure 59
9.2 Polishing 60
9.3 Electron beam evaporation 61
9.4 Previous experimental work 61

10 Electrical characterization techniques **63**
10.1 Current-voltage measurements 63
10.2 Capacitance-voltage measurements 64

11 Results **66**
11.1 Schottky contact deposition 66
11.2 R_s and η from current-voltage data 71
11.3 Evaluation of capacitance-voltage data 73

12 Discussion **76**
12.1 Effects of the surface topography 76
12.2 Effects of the lithium concentration 77
12.3 Effective donor concentration 77
12.4 Interfacial layer 78
12.5 Charging effect 78

III Conclusion and suggestions for future work **80**

13 Summary **81**

13.1 Conclusion 81

13.2 Future directions 82

IV Appendices **84**

A Lithium depth profiles **85**

B Typical IV and CV results **88**

References **93**

1 Introduction

Nothing is as simple as we hope it will be.

– Jim Horning

ZnO has been an integral part of the industry for quite some while, with research stretching back to as early as 1935 [1]. It is used in paints, cosmetics, plastics and pharmaceuticals, to name just a few [2]. Recently, access to high quality samples and its properties like ultra violet (UV) absorbance, wide direct band-gap, piezoelectricity and luminescence at high temperatures, have paved the way for renewed interest in ZnO, subsequently resulting in over 3000 publications only in 2006 [3]. It is regarded as an excellent material for photonic and optoelectronic devices, like UV-LEDs and lasers [4]. It is also attracting attention for its application to varistors, high density data storage systems, piezoelectric transducers, and recently also as transparent high power electronics and as window material for solar cells and displays [5, 6]. In addition, ZnO does have a potential for use in space applications because of its high radiation hardness.

ZnO has two major advantages over today's industry standard – GaN: (i) Larger exciton binding energy of 60meV at room temperature (RT=300K), which is higher than the effective thermal energy at RT (26 meV); And (ii) the ability to grow high quality crystals – which is still somewhat an issue for GaN.

Despite its huge potential there is one particular hurdle that needs to be mastered: p-type doping. Today, n-type doping is relatively easily attained through dopants

like aluminium and gallium, but reliable p-type doping is very difficult to achieve. Maximum hole concentration of 10^{19}cm^{-3} and low hole mobility of 5-15cm^2/Vs, compared to typical electron mobility of 200cm^2/Vs, have been reported [7], but a problem with the p-doping is that it typically vanishes within days or weeks [8]. However, these and other recent progresses in p-doping, especially with group-V elements, take us close to realizing p-n homojunction LEDs.

Aside from the issue with doping, Schottky diode formation on ZnO is also challenging. Good quality Ohmic and Schottky contacts are essential for device manufacturing and a range for experimental characterization techniques. Today, good Ohmic contacts are relatively easy to make with Al and Ti [5]. However, many Schottky contacts suffer from high reverse current, high series resistance and low Schottky barrier. Difficulty in reproducing the results and varying results in the same prepared batch, also indicate that surface states are a problem [2].

Thesis overview

This thesis is divided into two main parts: (i) "Lithium content and surface topography after annealing" and (ii) "Palladium Schottky contacts on hydrothermal ZnO". First (i) we will examine the behaviour of Li concentration in HT ZnO after isochronal annealing at temperatures ranging from 600°C to 1600°C . The resistivity and surface topography of the samples are also investigated. Based on these results, we tune the resistivity, the Li concentration and the surface roughness before depositing Pd Schottky contacts (ii). Each part is structured to have its own theoretical background, experimental details and techniques, results and discussion. At the end of the thesis conclusion and future directions are presented.

Part I

Lithium content and surface topography after annealing

2 Background

It is possible to store the mind with a million facts and still be entirely uneducated.

– Alec Bourne

Topics touched upon in this chapter are the general semiconductor theory and crystal defects. The theory presented here is well established and can be found in numerous books and articles, e.g. Refs. [9, 10].

2.1 General semiconductor theory

In a theoretically, perfect crystalline structure all atoms are arranged in a repeating fashion producing a flawless lattice. The smallest cell needed to describe the entire lattice is called a unit cell (figure 3.1). This orderly arrangement of atoms gives rise to a periodic Coloumb potential, which sets restrictions on the energy levels an electron can occupy. Regions where no solutions for so-called *Bloch function* exist form forbidden energy bands or band-gap with energy E_g. The size of this band-gap determines if the material is a metal, a semiconductor or an insulator (see figure 2.1).

All electrons having larger energy than the upper edge of the band-gap are free to move around in the crystal as a response to an external electrical field. These

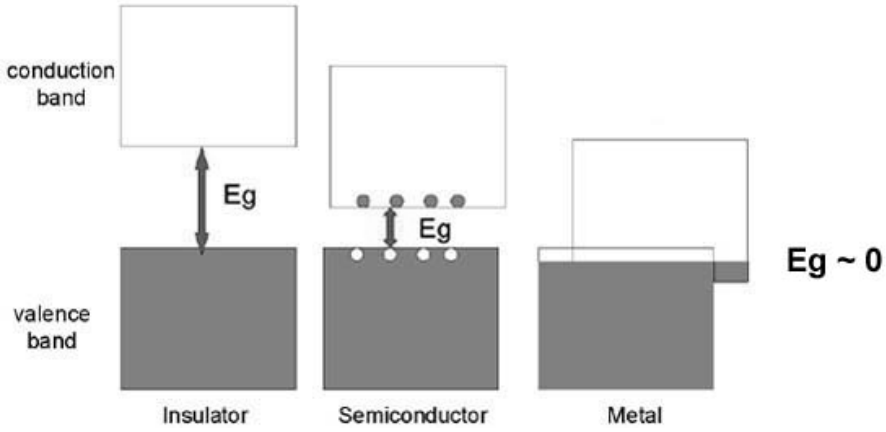

Figure 2.1: Schematic overview of the difference between an insulator, a semiconductor and a metal. Figure adapted from Ref. [11].

energies are collectively called the conduction band (CB). The bound energy states below the lower edge of the band-gap form the valence band (VB). Electrons can be excited from the VB to the CB, leaving behind empty states called holes. The carrier transport is described by electrons in the CB and holes in the VB. An electron in the CB can also recombine with a hole in the VB, annihilating a so-called electron-hole-pair (EHP).

Any periodic lattice can be given as a reciprocal lattice. In the reciprocal space, if the minimum of the CB is directly above the maximum of the VB (they occur at the same wave number $\vec{k}$), then the semiconductor is said to have a *direct* band-gap. If the maximum and the minimum do not occur at the same $\vec{k}$, then it is said to have an *indirect* band-gap.

Electrons in solids obey *Fermi–Dirac* distribution which gives the probability $f(E)$ of an orbital at energy E being occupied in an ideal electron gas, and is given by

$$f(E) = \frac{1}{1 + \exp\frac{E - E_F}{kT}} \tag{2.1}$$

where k is the Boltzmann's constant (see table 2.1) and T is the temperature in kelvin. Fermi level E_F shows that an energy state at this energy has $f(E_F) = 1/2$ probability of being populated. It also implies that at zero kelvin every available state up to E_F will be filled with electrons, and all states above this will be empty.

In an intrinsic material the Fermi level is usually in the middle of the band-gap. N-type material have the Fermi level closer to the CB, while in p-type material E_F is closer to the VB, corresponding to an excess of electrons and holes, respectively.

If E_F is several kT from the edge of the bands (low thermal excitation), the charge carrier densities in the CB and VB can be given by

$$\begin{aligned} n &= N_c f(E_c) \approx N_c \exp(-\frac{E_c - E_F}{kT}) \\ p &= N_v(1 - f(E_c)) \approx N_v \exp(-\frac{E_F - E_v}{kT}) \end{aligned} \tag{2.2}$$

respectively, and $N_{c,v}$ is the effective density of states in the CB and VB, respectively, given by

$$N_{c,v} = 2(\frac{2\pi m^*_{n,p} kT}{h^2})^{3/2} \tag{2.3}$$

$E_{c,v}$ is the energy at the edge of each band, $m^*_{n,p}$ is the electron and hole effective mass, and h is the Planck's constant.

Name	Description	Value
ε_{ZnO}	ZnO relative permittivity	8.91
ε_s	ZnO permittivity	7.89×10^{-13}Fcm^{-1}
m^*_n	Electron effective mass	$0.24m_0$
k	Boltzmann's constant	1.380×10^{-23}J/K
q	Electron charge	1.602×10^{-19}C
A^*	Richardson's constant	32AK^{-1}cm^{-2}
h	Planck's constant	6.626×10^{-34}Js

Table 2.1: Material property of ZnO and some constants [2].

2.2 Crystal defects

Even though semiconductors today can be made with very few unintentional defects, they are still not perfect. Thermodynamically, a completely perfect crystal is not energetically favourable. So the goal is not to make a flawless crystal, but

rather to reduce *unintentional* defects and impurities as much as possible. Defects, intentional or unintentional, can extend from zero to three dimensions – point-, line-, plane- or volume-defects. Some 0- and 1-dimensional defects are showed in figure 2.2.

Introducing foreign elements is called doping and can create new energy levels. Electrically active defects introduce energy levels within the band-gap, where they can trap, emit or recombine electrons and holes. Defects creating energy levels outside the band-gap are electrically inactive, but can still influence the mobility of the electrons and holes [12]. Levels close to either of the bands are referred to as shallow levels, while closer to the middle of the band-gap are called deep levels. Shallow levels can be introducing in e.g. silicon (Si) by doping with, among others, phosphorus (P) and boron (B), giving rise to donor and acceptor levels (n-type and p-type), respectively.

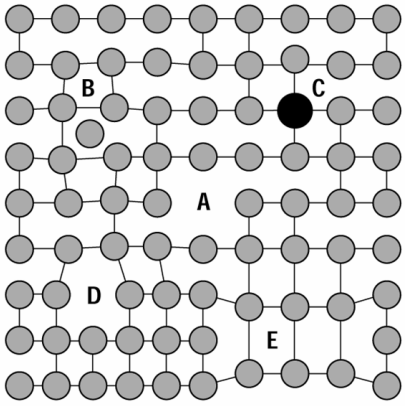

Figure 2.2: Some 0- and 1-dimensional defects. (A) Vacancies, (B) self-interstitials, (C) substitutional impurities, (D) edge dislocations, and (E) dislocation loops. Figure adapted from Ref. [13].

The site which a foreign element occupies in a crystal is very important to its electrical contribution. In the Si-example above, both P and B are substituted for Si. In two elemental semiconductors like ZnO, a dopant can either substitute for zinc (Zn) or oxygen (O) or position itself interstitially depending on what is more energetically favourable. In this thesis we will me concentrating on Li, which is known to give a donor level if substituted with either zinc (Li_{Zn}) or oxygen (Li_O),

but acceptor level if in an interstitial position (Li_i). This makes it more difficult to band-gap engineer a two elemental semiconductors than an elementary one.

3 Basic review of ZnO

Copy from one, it's plagiarism; copy from two, it's research.

– Wilson Mizner

This chapter will give a basic overview of the crystalline structure, growth and doping of ZnO. We will also give a short review of lithium.

3.1 ZnO crystal

The reader is referred to Refs. [2, 14] for a more in depth review of the ZnO crystal structure.

ZnO has a wurzite crystalline structure at ambient pressure and temperature, as shown in figure 3.1a. The Zn^{2+} ions are in a centre of a tetrahedral created by O^{2-} ions, and visa versa. Since this means that the structure does not have inversion symmetry, the crystal exhibits crystallographic polarity. This polarity gives the structure, among other things, its spontaneous polarization and piezoelectricity.

The convention is that the positive z direction points along [0001] axis from the face of the O-plane to the face of Zn-plane. In other words, $(000\bar{1})$ is said to have O-polarity or is the O-terminated face, since the bonds are going from the anion

(O) to the cation (Zn) along the c direction. By the same argument Zn-polarity is defined as the (0001)-plane. Other common faces are the non-polar $(11\bar{2}0)$ and $(10\bar{1}0)$ planes. In this thesis we will be examining the (0001)- and the $(000\bar{1})$-plane only, and they will be referred to as the Zn- and O-faces, respectively. The calculated lattice parameters are in good agreement with the measured ones. The a parameter range from 3.2475 to 3.2501Å, and the c parameter from 5.2042 to 5.2075Å [15].

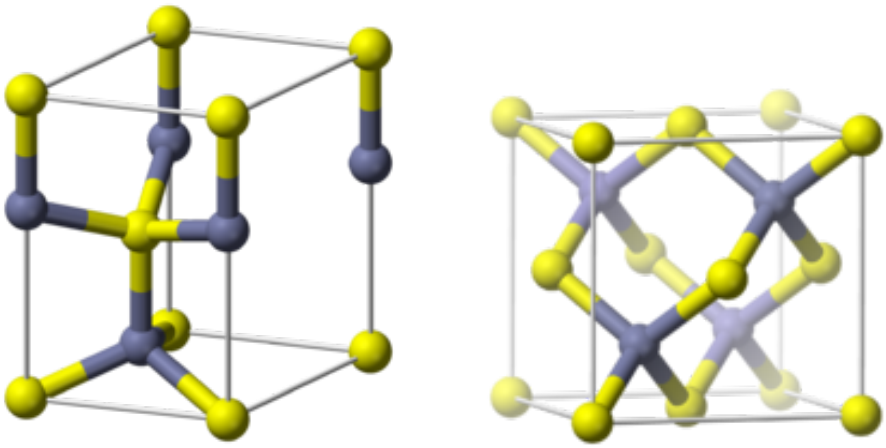

(a) **(b)**

Figure 3.1: (a) Wurtzite and (b) Zinc blende unit cell. The yellow spheres are oxygen atoms and the blue ones are zinc.

w-ZnO can be transformed into rock salt ZnO by applying a pressure of 10-15 GPa. It is also known to have a zinc blende structure (figure 3.1b), but this is only achieved by growth on cubic structures. Calculations have shown that there may be a fourth phase, cubic caesium chloride structure. Theoretically, it can be achieved at extremely high temperatures, but this has not been confirmed experimentally [2].

3.2 Lithium

The name Lithium originates from the Greek word Lithion meaning stone. It is a group-I alkali metal and the 33rd most abundant element on Earth [16], and under

standard conditions it is the lightest metal. As with other alkali metals, it has one valence electron, making it highly reactive and corrodes quickly in moist air.

Li has the highest specific heat capacity of all the solids making it well suitable for heat transfer applications. Its high electrochemical potential, light weight and ability to transfer a high current density makes it an important ingredient in batteries. Li salts are also used is pharmaceuticals as mood stabilizers.

Most abundant Li isotope is the ^{7}Li with 92.5% abundance. Seven other isotopes have been characterized, but in this thesis only ^{7}Li will be investigated. Refer to table 3.1 for properties of Li.

Atomic number	3
Atomic weight	$6.941u$
Electron configuration	2.8.1
Melting temperature	180°C
Boiling temperature	1342°C

Table 3.1: Various properties of Li [17].

3.3 Doping of ZnO

As mentioned previously, ZnO has a huge potential for various device applications, but first we have to attain high quality p- and n-doped ZnO. As with many other wide band-gap compound semiconductors, doping remains a non-trivial issue.

Most of the information in this section is gathered from Refs. [5, 15, 18].

3.3.1 n-type doping

w-ZnO is naturally (and unintentionally) a n-type semiconductor. There is some dispute over what the main reason is for this n-type behaviour. For a long time it was thought to arise from oxygen vacancies (V_O) and/or zinc interstitials (Zn_i).

Later theoretical studies have suggested that both V_O and Zn_i have too high formation energies, and thus cannot be the main reason for the n-doping [19]. In addition V_O is a deep donor, not shallow as previously thought [20, 21]. Even though these native defects are not major contributors to the n-type conductivity as isolated defects, they can however, still have an impact as complexes.

Some reports suggest that hydrogen is the main cause of n-doping [22]. Hydrogen acts as shallow donor independent of the Fermi energy level (not amphoteric as in Si), and has very low formation energy. However, since group-III elements also act as shallow donors, and in many cases are Al and Ga more abundant than hydrogen. It indicates that hydrogen cannot be the sole reason for the n-doping [18]; Even though, it still remains one of the most important n-type dopants because of its presence during almost all the growth processes.

Reproducible and reliable n-type doping of ZnO is relatively easy. Group-III elements Al, Ga and In substituted for Zn (see table 3.2), and group-IV elements Cl and I as substituted for O can be used as n-type dopants. Myong et al. [23] have been successful in making highly conductive Al-doped ZnO film with minimum resistivity of $6.2 \times 10^{-4}\Omega$cm.

Element	Structure	Energy $E_c - E$ [meV]	Ref.
Al	Al_{Zn}	65/53	[24, 25]
B	B_{Zn}		[3]
Cr	Cr_{Zn}		[3]
Ga	Ga_{Zn}	54.5	[25]
H	H_i	37/46	[24, 26]
In	In_{Zn}	63.2	[25]
Li	Li_i	1400	[18]
O	V_O?	300	[24]
Zn	Zn_i	46	[24, 27]

Table 3.2: Overview of some donors in ZnO. Table adapted from [3].

3.3.2 p-type doping

The difficulty in producing p-type ZnO is reflected by the fact that there were no reports of p-type ZnO until 1997 [28]. From then till now, nitrogen remains the most studied acceptor dopant. Its ability to give acceptor levels at 110meV when resided at oxygen sites (N_O) (see table 3.3), and solubility of up to $10^{19}cm^{-3}$ [6] make it a good candidate for n-doping. Since it also has similar size as oxygen, N_O gives bonds close to the ideal oxygen bonds (see table 3.4), resulting in less lattice strain and thus fewer defects. However, problems with low hole mobility and few active acceptors remain. Measurements done by Look et al. [15], show a nitrogen concentration of $10^{19}cm^{-3}$, while only low-$10^{15}cm^{-3}$ were active.

Element	Structure	Energy $E - E_V$ [meV]	Type	Ref.
Ag	Ag_{Zn}/Ag_i	200	Amphoteric	[29, 30]
As	As_{Zn}		Donor	[3]
Cu	Cu_{Zn}	380/190	Deep acceptor	[30, 31]
Li	Li_{Zn}	200	Deep acceptor	[18]
N	N_O	110	Acceptor	[32]
Na	Na_{Zn}	600	Deep acceptor	[3]
P	P_O		Acceptor	[7]

Table 3.3: Overview of some acceptors in Zno. Table adapted mainly from [3].

The rest of the group-V elements As, P and Sb also work as p-type dopants, which is quite surprising; Since their larger radii would suggest much strain on the lattice, and thus lower solubility. However, reports have shown As-doping giving concentration of mid-$10^{19}cm^{-3}$ and an acceptor concentration of $10^{19}cm^{-3}$ [3]. This may be explained by As not residing as As_O, but rather as much more complex acceptor-like defect.

Native defects like O_i and V_{Zn} should theoretically be acceptors, and negatively charged V_{Zn} does contribute some to the acceptor concentration. However, experimentally little is known about O_i.

	Element	Bond length (Å)	E_i (eV)
Group–I	Li	2.03	0.09
	Na	2.10	0.17
	K	2.42	0.32
Group–V	N	1.88	0.40
	P	2.18	0.93
	As	2.23	1.15

Table 3.4: Calculated values for bond length to nearest neighbour and defects energy level above the VB created from substituting into the lattice. Ideal Zn–O bond length is determined to be 1.93Å. Table adapted from [14].

3.3.3 Lithium doping

The solubility of lithium in ZnO is very high, and experiments have shown up to 30% of Zn sites can be occupied by Li [33]. As we will discuss in section 3.4, hydrothermal growth method can incorporate large concentration of Li in the ZnO crystal. Combined with the fact that Li_{Zn} give an acceptor levels, makes lithium very interesting as acceptor. An obstacle is interstitial lithium, Li_i, which gives compensating deep donor levels. Li_{Zn} and Li_i levels are thought of being 0.2eV and 2.0eV above VB, respectively, resulting in semi-insulating material when doped with Li. A reason for this is that the small size of Li makes it more prone to be in the interstitial position than the substitutional one. As table 3.4 shows, Li bond are bigger than the ideal bond, generating compensating donor-like vacancies. Doping with Li is also known to increase the resistivity in ZnO; For acoustical applications Li has been used to increase ZnO resistivity up to $10^{12}\Omega$cm [3].

Wardle el at. [18] has examined various other positions that Li may occupy. Theoretically Li can be on a O site, but relaxation of Li_O is very unstable and can best be described as a V_O–Li_i complex. This would become a triple donor, since V_O is a double donor. The formation energy for a V_O–Li_i complex is too high for it to be in any significant concentrations.

Li may also form a Li_{Zn}–Li_i complex. This complex can be seen as a distorted Li_2O unit cell within the hexagonal ZnO, and is electrically inactive. Incorporation of Li_2O may be the reason for the enhanced ferro electrical properties seen at high

Li doping, which was previously assigned to dilation of the Li–O bond.

The most stable formation seems to be a Li_{Zn}–H complex with a high binding and a low formation energy. If H increases the intake of Li_{Zn}, then the acceptors may be activated by annealing. A similar step can be suggested for a ZnO grown with absence of H. Then the Li_{Zn}–Li_i complexes would be abundant, and an annealing step could reduce the concentration of Li_i.

There are however, theoretical indications of a limiting factor even in Li_i- and H-free samples, and only Li_{Zn} present. A donor-like complex is then energetically favourable, created by breaking up two Zn–O bonds to make a O–O bond. This indicates that there may be an upper-limit to the p-type carrier concentration that can be obtained from Li doping.

3.4 ZnO growth methods

Some few growth methods of ZnO crystals are presented here, and the reader is referred to e.g. Refs. [2, 6] for other methods.

Since ZnO has been around for so many years in the industry, ZnO powder is easy to produce. It is made from the combustion of vapour coming from distillation of metallic zinc, a so-called French or dry process. In order to grow higher purity samples, other methods have to be used. One of these is the pressurized melt growth method. Here ZnO is heated under an oxygen overpressure of close to 5MPa, resulting in a stoichiometric crystal. Big ingots[1] with low defect concentrations can be made in a short time (up to 1cm/h). However, it remains a problem to make large grain size with this method.

Samples used in this report were grown hydrothermally, which is known to give higher purity samples than by pressurized melt growth method. Crystal growth is achieved by convection between two different ZnO containing zones: a dissolution zone and crystal growth zone. These are kept at high pressure (up to 140MPa) and at a temperature difference $\Delta T \approx 20 - 80^{\circ}$C, with the crystal growth zone being at the lower temperature. Starting ZnO is usually in an aqueous solvent of

[1] Up to a diameter of 5.5inch and kilogram sized ingots have been reported [6].

KOH and LiOH at 270-350°C, and incorporation of impurities like lithium and potassium from the solvent is a problem. Typically, the incorporated Li is at 10^{-2}-10^{-4}wt.%, and other contaminations like Cu, Mg, Si, Fe, Mn and Ag are at 10^{-3}-10^{-4}wt.%. Other disadvantages with HT growth method are the slow growth rate (0.05-0.3mm/day) and the complex setup needed (e.g. Pt liner for reducing the contamination).

4 Sample preparation

Basic research is what I am doing when I don't know what I am doing.

– Wernher von Braun

4.1 Experimental procedure

The samples used in this report were two single crystalline HT grown 1x1cm^2 ZnO samples purchased from Goodwill in Russia (see table 4.1). As mentioned previously, HT grown ZnO is synthesized in, among other things, LiOH, which gave the sample a high residual Li concentration and made them highly resistive.

The crystal orientation was as shown in figure 4.1. The oxygen terminated face is the $(000\bar{1})$-plane, while zinc terminated is (0001)-plane. Most of the impurity depth profiling done in this report took place on the oxygen face. If nothing else is specified, the surface in question will be the O-face.

The behaviour of Li concentration was investigated after annealing at temperatures ranging from 600°C to 1600°C. We also examined the effects on the resistivity and the surface topography. Two 1x1cm^2 wafers of ZnO were divided into four equal sized samples using a diamond saw (figure 4.1). The samples were labelled as *1, 2, 3, 4* and *a, b, c, d*, and were annealed at a constant temperature. A ceramic

Purity	$> 99.99\%$
Dimensions	10x10x0.5mm^3
Electrical resistivity	500-1000Ωcm
Specific heat	$\approx$ 525J/kg
Band-gap [a]	3.37eV
Exciton binding energy [a]	60meV
Both sides epi polished	$R_a < 1.0$nA
Lattice mismatch with $(000\bar{1})$ GaN	$< 2.2\%$

[a] At room temperature

Table 4.1: Specifications of the ZnO samples in use [34].

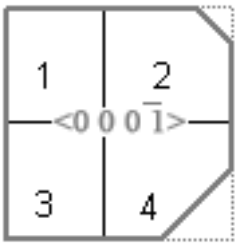

Figure 4.1: Sample schematics with the O-face on top. Samples were cut into smaller pieces, denoted by numbers $1-4$ (or $a-d$ for the second sample) [34].

boat was loaded with the samples and inserted into a pre-heated furnace. After one hour of annealing time, the samples were taken out and cooled passively by the ambient temperature. For cost reduction, samples 1–3 were each annealed for a total of three times, with 300°C interval between the temperatures, and for 1h every time (see table 4.2)[1]. It could go up to one to two weeks before the samples were annealed again at higher temperatures. Samples a and b were heated only once. The rest of the samples (and some new ones) were used for Schottky diode deposition explained in the next part of the report.

Sample	Temp. 1 [°C]	Temp. 2 [°C]	Temp. 3 [°C]
1	600	900	1200
2	700	1000	1300
3	800	1100	1400
a	1500		
b	1600		

Table 4.2: Overview of which temperatures each sample was annealed. Treatment time was 1 hour at each temperature.

After each annealing step, Li profile of every sample was measured with secondary ion mass spectrometry and resistivity with four-probe point measurement. In addition, the surface roughness was measured after high temperature anneals with a white light interferometer (WLI). See figure 4.2 for an overview of the experimental procedure.

Each sample was cleaned with organic solvent before annealing; Five minutes in acetone, ethanol and de-ionized water, all in ultrasonic bath, then blown dried with N_2. This cleaning step was intended to remove contaminations on the surface, especially InGa residuals after the four probe point measurements (section 5.2).

[1] We predicted that only the absolute Li concentration would be affected by multiple anneals, not the behaviour of the Li concentration versus depth. We will show later that it was a reasonable prediction.

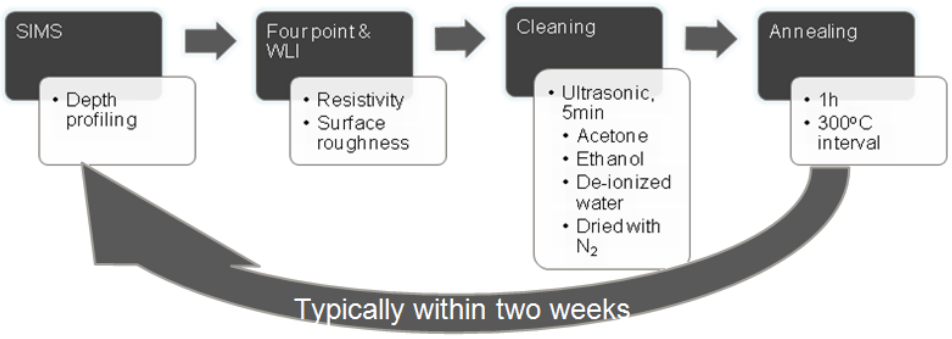

Figure 4.2: Overview of the experimental procedure.

5 Experimental characterization techniques

If you are out to describe the truth, leave elegance to the tailor.

– Albert Einstein

5.1 Secondary ion mass spectrometry

5.1.1 Overview of SIMS

Secondary Ion Mass Spectrometry (SIMS) is a characterizations technique for thin films and surfaces up to a few tens of microns. It uses a beam of primary ions to bombard the sample, and results in a sputtering process where only a small fraction of the emitted particles are ionized. These ionized particles, or secondary ions, are then filtered out by energy and mass before hitting a detector (see figure 5.1).

Our system used O_2^+ or Cs^+ as source for the primary beam. The selection of the source was dependent on the required polarity of the secondary ions. We mainly used the oxygen source in our experiments. Absolute detection limit of SIMS depends on several factors, but can be as low as sub-ppm over only a handful of atomic layers [35]. A downside of the SIMS is that it is destructive – it generates a crater on the sample (see figure 5.2) and affects the quality of any future deposited Schottky diodes.

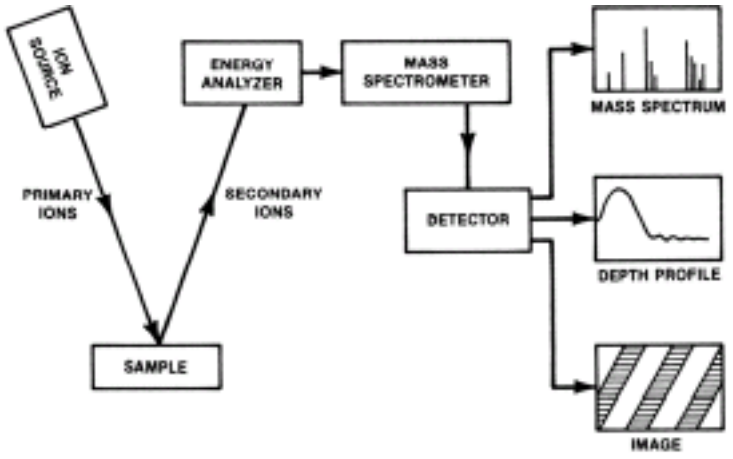

Figure 5.1: Schematic overview of the SIMS [35].

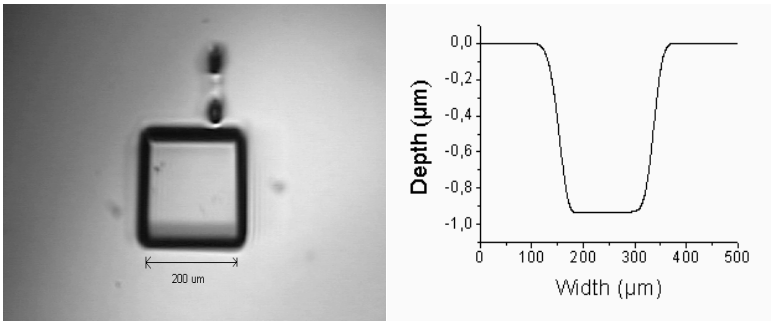

(a) **(b)**

Figure 5.2: (a) A 200x200μm crater made my a primary beam of 200nA current, and sputtering time of 700s. The two dots over the crater are made for identifying the correct crater for later times. (b) Profile of the crater obtained with a stylus profiler [36].

The SIMS can give result in different ways; Most common are depth profiling, mass spectrum and the ion image. Mass spectrum shows the abundance of various isotopes. Ion image shows the distribution of various species on the surface – good for investigating homogeneity. The method most used in this report was the depth profile. It gives counts per second (intensity) versus time and needs to be calibrated to give concentration versus depth (see section 5.1.2).

Besides measuring the actual isotope, one also need to monitor a so-called matrix or a reference signal. This is to determine if the measurement is reliable and if the isotope signal is real. Matrix signal has to be constant, and is chosen to be an element that is abundant in the sample.

If the sample is highly resistive, one can encounter a charging effect which disturbs the secondary ion beam. The high resistivity accumulates the charge from the primary ions around the targeted region. After a few moments this charge becomes big enough to compensate the bias put on the sample for extracting the secondary ions. One way to counteract this problem is to use an e-gun, which bombards the sample with electrons, together with the primary ion beam. This may in some cases heat up the sample and give unintentional annealing, and thus needs to be used with care.

5.1.2 Calibration of SIMS data

Figure 5.3 shows a typical plot obtained from SIMS measurement and one that is calibrated. To transform intensity versus time into concentration versus depth one normally assumes a linear erosion rate when the kinetic energy of primary ions is kept at constant. The depth of the crater has to be measured afterwards, and in our case was done with a *Veeco Dektak 8 stylus profiler*. In addition, one has to have a reference sample with known implantation dose of the element in question. The reference sample that was used for this report had a dose of $2.5\times10^{14}\text{cm}^{-2}$.

We assume a linear erosion rate, which is given by

$$\text{Erosion rate} = \frac{\text{Depth}}{\text{Time}} \tag{5.1}$$

Where *depth* is the measured depth of the crater, and the *time* is how long the

measurement lasted. The total number of counts are given by

$$\text{Counts} = \int_0^t I(t')\partial t' \tag{5.2}$$

Where $I(t')$ is the intensity. Background concentration and surface abnormalities are removed for more accurate calculations. E.g. in the case of figure 5.3, the integration was taken in the range $t \in [100s, 1700s]$. Now the calibration constant is given by

$$\text{Calibration constant} = \frac{\text{Dose}}{\text{Counts} \times \text{Erosion rate}}$$

We can use this constant to change intensity to concentration by

$$\text{Concentration} = \text{Calibration constant} \times \text{Intensity}$$

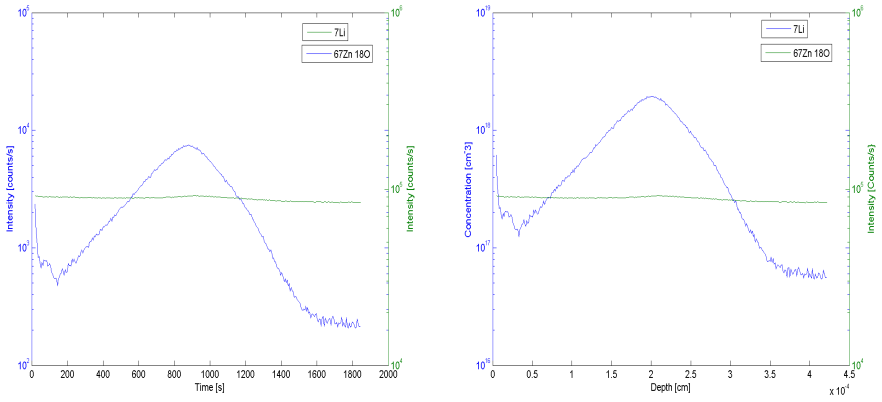

(a) **(b)**

Figure 5.3: (a) Non-calibrated and (b) calibrated profile of a ZnO reference sample with ^{7}Li implanted at a dose of $2.5 \times 10^{14}\text{cm}^{-2}$. $^{67}\text{Zn}^{18}\text{O}$ molecule was used as the matrix signal for this measurement. For the rest of this report the matrix signal profiles are omitted.

5.2 Four probe point measurement

After each anneal samples' resistivity were measured with four probe point measurements. The four point measurement is preferred over the two point, because with two probes there are no means to distinguish between the measured resistance and the resistance associated with the probing contacts [37].

The four probe point measurement uses two probes for current measurement, while the other two measure the voltage. By neglecting the resistance associated with the two voltage probes (which is a reasonable approximation), one can obtain fairly accurate numbers for the resistivity ρ, given as

$$\rho = 2\pi KP\frac{V}{I} \tag{5.3}$$

where V and I are the measured voltage and current, respectively. $K \approx 0.52$ is a correction factor and depends on the ratio between the sample thickness E and the probe spacing P, which in our case were 0.5mm and 0.7mm, respectively. From the resistivity measurements an estimate of the electron concentration n and hole concentration p can be done by

$$\frac{1}{\rho} = \sigma = q(\mu_n n + \mu_p p) \tag{5.4}$$

where $\mu_{n,p}$ is the electron/hole mobility, q is the electron charge and σ is the conductivity.

Our samples had high resistivity, so the probes were dipped in eutectic InGa for improved contact. Residual InGa was later removed by the organic solvent cleaning steps as mentioned in section 4.1.

5.3 White light interferometer

White Light Interferometry (WLI) is a powerful technique for non-contact and reproducible measurements of surface topography. Almost any surface can be measured, even the ones with low reflectance – minimum of $\approx$2% reflection is required, and a measurement takes no more then a few seconds.

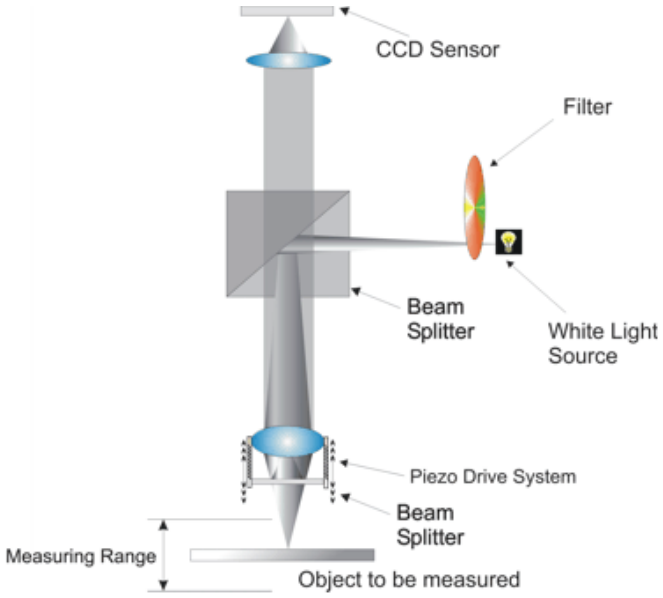

Figure 5.4: Schematic diagram of an WLI microscope. Figure adapted from [39].

The WLI instrument in use was a *Zygo NewView 6200*, and had a specified vertical resolution of < 0.1nm and lateral resolution of 2.19μm [38]. These numbers are at optimum operating conditions, which we unfortunately did not have. So a more modest estimate would be $\approx 0.5 - 0.6$nm and $\approx 3\mu$m in vertical and lateral resolution, respectively.

To explain how a WLI works, we will examine a simple system which utilizes two white lights. A beam from a white light source is split into two beams; One is reflected from the sample, the other one follows a known and constant optical path. Both beams are then combined in a so-called Mirau type interferometer arrangement [39], to create a pattern of light and dark fringes – a diffraction pattern. By changing the vertical distance between the sample and the objective (figure 5.4), the point where each pixel is at its brightest can be established (maximum constructive interference). The software can then calculate the relative height difference between each pixel. Calibrated against a reference sample (provided by the manufacturer), one can then obtain the absolute height difference between all the pixels, and thus create a 3D image of the surface.

6 Results

The most exciting phrase to hear in science, the one that heralds new discoveries, is not 'Eureka!' (I found it!) but 'That's funny...'

– Isaac Asimov

Both the profiling and the resistivity measurements were done on the O-face if nothing else is specified.

6.1 Lithium concentration measurements

Native Li levels in all the samples before annealing were constant as a function of depth at a level of $\approx 10^{17}\text{cm}^{-3}$, and it stayed at that level until annealed at $>900^{\circ}\text{C}$. At 1000°C the concentration fell dramatically by an order of magnitude to $\approx 10^{16}\text{cm}^{-3}$ (figure 6.1a). Further heating showed an accumulation of Li in the first few microns of the surface. At higher temperatures a wider plateau-like formation seemed to emerge (see figure 6.1b).

For depth profiles for all the samples, see appendix A.

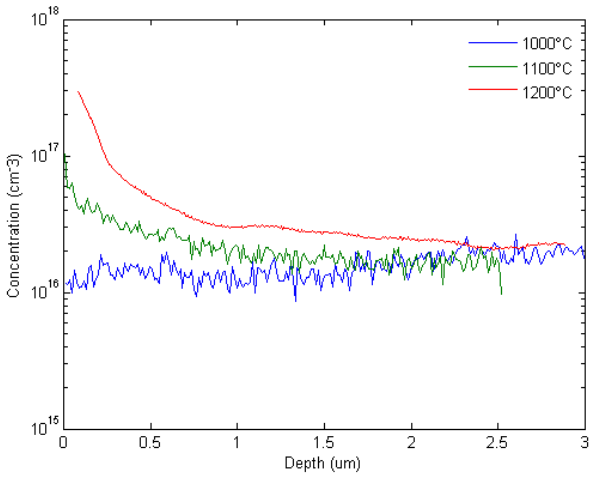

(a)

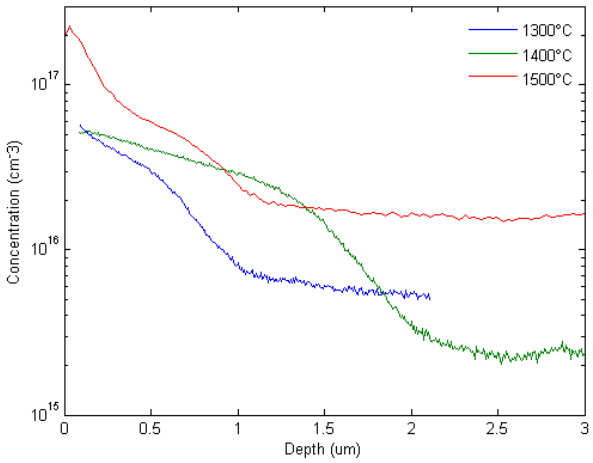

(b)

Figure 6.1: (a) Shows the low-10^{16}cm^{-3} Li concentration obtained from 1000°C-anneal and an accumulation occurring. (b) The accumulated Li is turning into a wider plateau-like formation. The 1500°C profile corresponds to a sample annealed once, while the others are from samples annealed multiple times (cf. table 4.2). This explains the higher Li concentration after 1500°C anneal.

6.2 Resistivity measurements

After every anneal the resistivity for each sample was measured with the four probe point method. This showed an increase in resistivity from unannealed to 600-800°C annealed samples, $\approx 10^3\Omega$cm to $10^5\Omega$cm, respectively. It then decreased several orders of magnitude to $\approx 0.5\Omega$cm at temperatures above 1300°C (see figure 6.2).

Eq.(5.4) can be written as eq.(6.1) for a n-type ZnO with low hole mobility.

$$\frac{1}{\rho} = q\mu_n n \tag{6.1}$$

From equations (2.2) and (2.3) the difference $E_c - E_F$ in eV, denoted ξ, can be calculated as

$$\xi = kT \ln \frac{N_c}{n} \tag{6.2}$$

If a mobility of 210cm^2/Vs at RT is assumed, which is a quite often quoted number in literature [2, 4, 40]. Then equations (6.1) and (6.2) give a carrier concentration of 5×10^{16}cm^{-3} and $\xi \approx 0.11$eV for a sample annealed at 1500°C with resistivity of 0.5Ωcm. For unannealed samples with resistivity of $\approx 10^3\Omega$cm, the calculations reveal a carrier concentration of 10^{13}cm^{-3} and $\xi \approx 0.35$eV. The latter are in good agreement with 2.3×10^{13}cm^{-3} reported by Look et al. [41], and with $\xi = 0.4$eV presented by Jacobi et al. [42] for an untreated sample.

6.3 Surface roughness measurements

Surface roughness, root mean square values (rms), of the samples were measured with WLI after they had been annealed. The final roughness was an average of two to three rms values from different locations, and each rms was from an area of 1.40x1.05mm^2. The roughness increased from $\approx$ 10nm for unannealed samples to $\approx$ 3500nm for annealing temperature of 1600°C. It was also apparent that the O-face was rougher than the Zn-face at temperatures above 1000°C (figure 6.3).

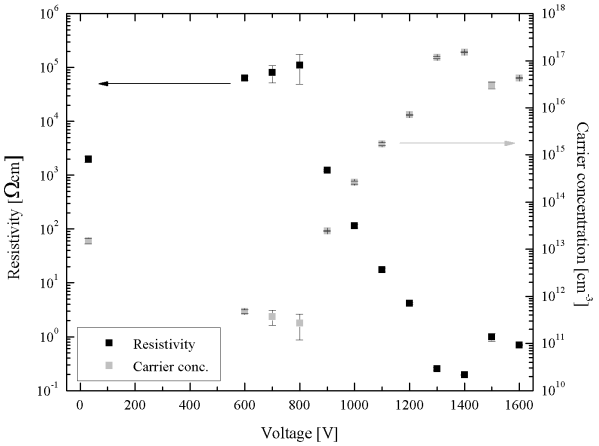

Figure 6.2: Measured resistivity and calculated donor concentration using eq.(6.1) versus annealing temperature. The samples at 1500°C and 1600°C are not annealed multiple times and probably therefore have higher resistivity. Annealing temperature of 30°C means unannealed samples.

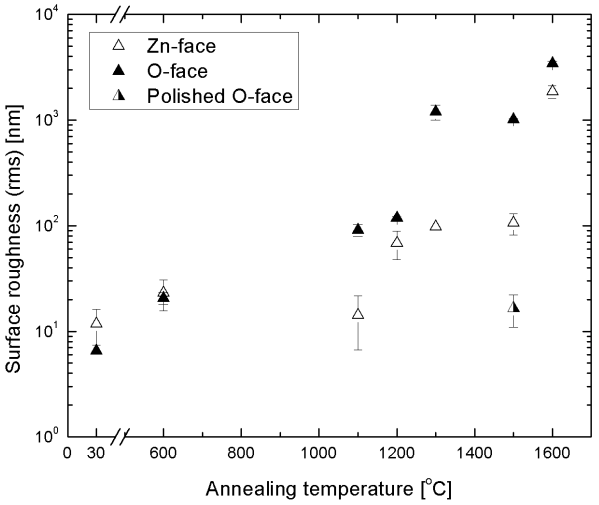

Figure 6.3: Surface roughness versus annealing temperature for both the O- and Zn-face.

Some samples were polished[1] and showed low rms values indicating seemingly flat surfaces - in reality they were not flat, but wavy. Their surfaces can best be described as a smooth landscape with no trees: This gave high peak-valley values (distance from lowest to highest point), but at the same time the root mean square fit was very good because of the lack of roughness (or trees in this analogy). It must also be stressed that the 1500°C-anneal created big pits, which could be as deep as several tens of μm. These pits were difficult to completely polish away and surface measurements exclude these pits. Estimated polishing depth was 50-60μm.

As seen in figures 6.4 and 6.5, there were big differences on the O-face of unannealed and high temperature annealed samples. At 1200°C the O-face had small "dents". These dents seemed to be localized, meaning that in some areas there were a high density of them, while in others few or none at all. This changed when annealed at 1300°C; Now they occurred very frequently all over the sample with the same density as the high density areas at 1200°C. At 1400°C the dents turned into big, deep pits.

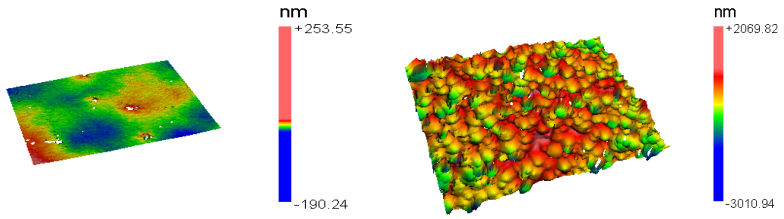

(a) **(b)**

Figure 6.4: (a) O-face of a new, unannealed sample. (b) Same surface after 1400°C anneal. Both figures are from an area of $1.40 \times 1.05\text{mm}^2$.

[1]The reason for the polish will be explained in chapter 9

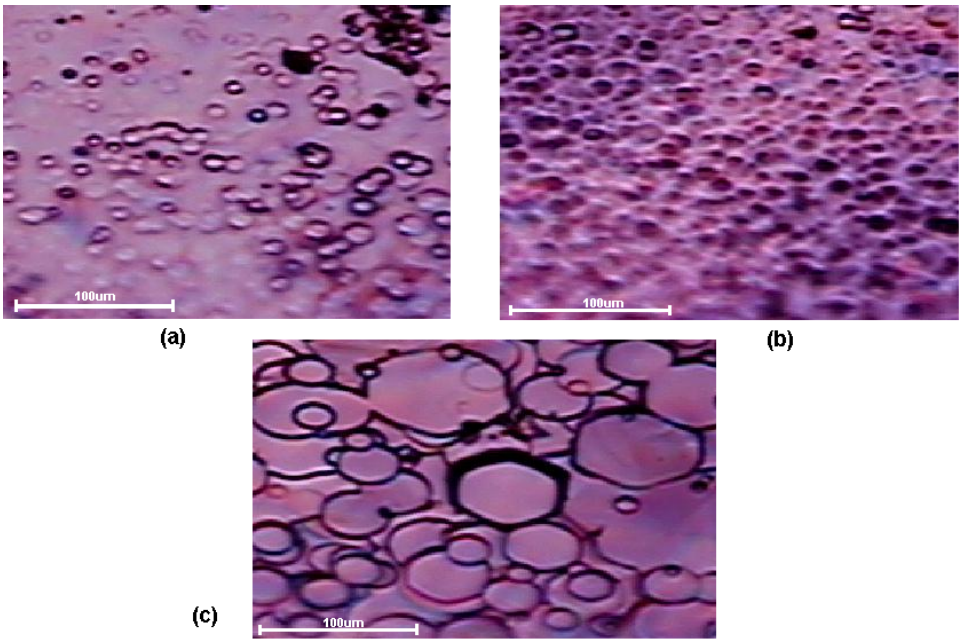

Figure 6.5: O-face surface of samples annealed at (a) 1200°C, (b) 1300°C and (c) 1400°C.

7 Discussion

Something unknown is doing we don't know what.

– Sir Arthur Eddington

7.1 Sample topography

As shown in figure 6.5 small pits exist on the O-face with diameter of $5-10\mu$m, turning into much bigger pits with diameter of up to 80μm after high temperature annealing. This transformation could be a result of line defects accumulating together to make a more energetically favourable defect structure, and thus creating wider and deeper pits. There is also a distinct difference in the shape of pits at 1300°C and at 1400°C, figure 6.5b and c, respectively. This may have been caused by Li reaching it's boiling temperature (cf. table 3.1), and in turn could have affected its the diffusion rate. Diffusion of oxygen could also have played a role. However, we can conclude that it is *not* from out-diffusion of zinc. Zn signal was used as matrix signal for most of our SIMS measurements and remained constant throughout.

A way to examine Li's role in making the craters would be to anneal a sample at 1500°C, and then polish at both sides. As we will show below, this will give a stable Li concentration of 10^{13}cm^{-3}. Now by annealing the sample again at 1500°C, we would expect fewer craters at the O-face since the sample has lower Li content *if* they are indeed caused by Li.

7.2 Lithium content

Our prediction that the multiple anneals with 300°C intervals would only affect the absolute concentration seems to be valid. As figure 6.1b shows, 1500°C-profile fits in well with the expected behaviour, although it is higher up in concentration.

The first signs of the Li concentration reduction occurred at 1000°C, falling a decade to a constant level. The biggest drop in the concentration occurred when treated at 1600°C. Bulk level fell from 10^{17}cm^{-3} to as low as mid-10^{13}cm^{-3} (figure 7.1). However, after 1h at 1600°C the sample started to evaporate, and was half the size than prior to the anneal.

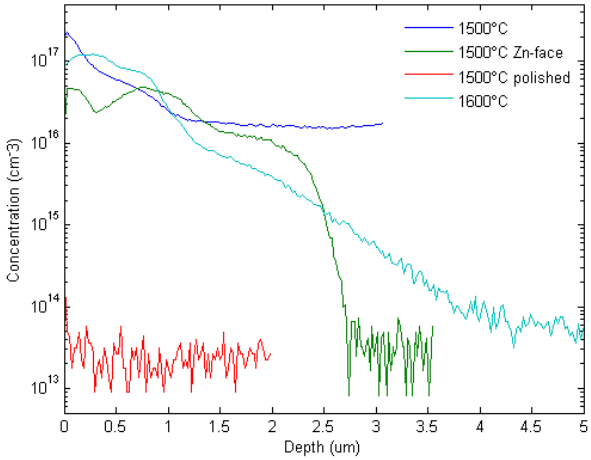

Figure 7.1: Li profiles of 1500°C at Zn-face, and from O-faces of 1500°C, polished 1500°C and 1600°C. Mid-10^{13}cm^{-3} is close to the SIMS' detection limit, therefore the big fluctuations.

As figure 7.1 shows, the stable bulk concentration of a sample treated at 1500°C is seemingly 10^{16}cm^{-3}. After a 50-60μm surface polish of the sample, the Li concentration showed mid-10^{13}cm^{-3}. This can only mean that the actual bulk concentration at high temperatures is evidently much lower than what appear in the first ten or so microns show. An estimate would be that the stable level is as deep as 30-40μm from the O-face. Also, the bulk level at high temperatures seemed to be much shallower on the Zn-face than on the O-face; 3μm on the Zn-face for 1500°C sample, compared to an estimated depth of $\approx 30-40\mu$m at the O-face.

Figure 7.2 shows a collection of measurements obtained for a sample annealed at 1500°C. We can only speculate on if the shape of the profile at the O-face continues to decrease slowly or at some point falls abruptly as at the Zn-face. However, this behaviour indicates that the out-diffusion of Li seems to be dependent on the surface polarity.

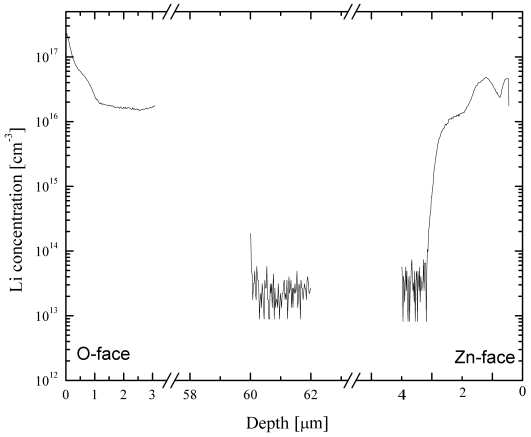

Figure 7.2: Collection of measurements of Li concentration on the same sample, annealed at 1500°C. Regions on the left and on the right (closest to the surfaces) were measured after the anneal. Region in the middle was measured after an estimated O-face-polish of 60μm.

Since Li accumulates at both surfaces, it is fair to assume that Li diffusion barriers exist at both sides. However, the total accumulated concentration varies much from the O- to the Zn-face (figure 7.2). Allen et al. [43] have shown that the spontaneous polarization in as-grown HT ZnO results in a neutrally charged bulk, while the O- and Zn-face are positively and negatively charged, respectively. This would influence the diffusion of the two main Li defects, Li_{Zn}^{-} and Li_{i}^{+}. Wardle et al. [18] have calculated that Li_i has a low activation energy for diffusion, which intuitively gives sense because of Li's small size. Therefore, Li_i diffusion through the negatively charged Zn-face would be relatively easy, and thus show a shallow/small accumulation. On the other hand, Li_{Zn} is expected to diffuse to the positively charged O-face, and a higher diffusion energy than Li_i is thought to give the observed long accumulation tail. The longer tail may also suggest higher density of Li traps at the

O-face than at the Zn-face.

A possible examination method of the Li diffusion at the two faces would be to first lower the Li concentration with a 1500°C anneal, then polish the samples, before implanting a high dose of Li on both the Zn- and O-face on two different samples. This will give a high Li-peak with low background concentration in each sample. Now by annealing the sample at high temperatures, Li diffusion of the two surfaces can be compared by examining the peaks, and by neglecting the influence of the remaining implantation-induced defects.

Annealing at temperatures higher than 1000-1100°C caused the samples to become somewhat inhomogeneous, although this was very difficult to observe. Li formed precipitates, resulting in areas with high concentrations. However, these areas were hard to find, and we did not observe them with the ion image mode of the SIMS. Only at a couple of occasions, by chance, we measured one of these Li-dense areas, as seen in figure 7.3. As these areas seemed to be so scarce, we do not believe that they affected the four point probe resistivity measurements, since the needles were pressed down on the sample and could easily penetrate the first microns. However, as we will show later, we do believe these Li-dense areas affected the quality of the Schottky diodes.

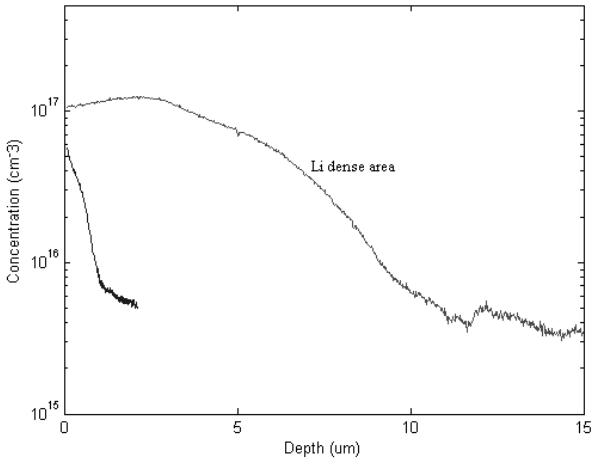

Figure 7.3: Both measurements were done on the same sample annealed at 1300°C, and show one of the Li-dense areas.

7.3 Sample resistivity

There seems to be a correlation between the average bulk Li concentration[1] and the sample resistivity over 800°C of annealing temperature, see figure 7.4. Below 800°C, no correlation was observed; In fact the resistivity increased with almost two decades from $2 \times 10^4 \Omega$cm to as high as $10^6 \Omega$cm, whilst the concentration remained nearly constant.

All hydrogen is known to diffuse out at temperatures of 500-600°C [44]. As Kassier et al. [45] suggest, a sharp increase in resistivity can be contributed to decomposition of Li_{Zn}–H complexes at the surface. In other words, annealing at 600°C activates acceptors like Li_{Zn} and other group-I elements at Zn-sites, thereby reducing the conductivity in a n-type ZnO.

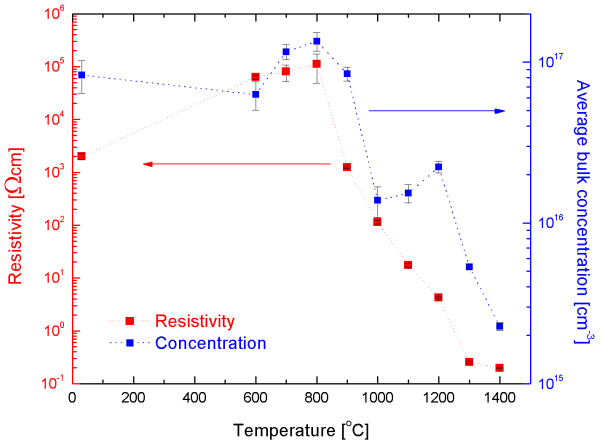

Figure 7.4: One can clearly see the correlation between the average bulk Li concentration and the resistivity for annealing temperatures above 800°C.

Above 800°C the concentration decreased from 10^{17} to 10^{15}cm^{-3} while at the same time resistivity fell *six* decades from 10^5 to $10^{-1}\Omega$cm. Lithium is sited mainly

[1] *The average bulk concentration* was calculated as the average Li concentration only over the area on the O-face where the concentration was constant and no deeper than 10μm (although the *actual* bulk level, as we have shown previously, could be much deeper in some cases).

as Li_i and/or Li_{Zn}, other sites are not expected to exist in any significant amount [18] . So reducing Li will reduce shallow Li_{Zn} acceptor levels and deep Li_i donor levels. Electrically, Li_{Zn} is more pronounced than Li_i because of it being much shallower, and thus in comparison, Li_i's influence on resistivity can be disregarded. We therefore speculate that the *increase* in the resistivity at temperatures below 800°C is mainly caused by breaking up Li_{Zn}–H complexes and activating Li_{Zn} in the bulk, and the subsequent the reduction in resistivity is mainly due to reduction in compensating Li_{Zn} acceptor levels in the bulk.

The sample annealed at 1500°C had a higher resistivity and a higher Li concentration than expected from 1400°C measurements because of the different number of anneals (figures 6.1b and 6.2). However, this fits in well with our observations of a correlation between Li content and resistivity when annealed at high temperatures. It also seems like $\approx 0.5\Omega$cm is the lower limit of the resistivity that can be obtained from simple annealing experiments, since 1300-1600°C anneals gave all approximately the same resistivity.

Part II

Palladium Schottky contacts on hydrothermal ZnO

8 Basic theory of Schottky diodes

There are no such things as applied sciences, only applications of science.

– Louis Pasteur

For device manufacturing it is essential that we are able to make both good Schottky and ohmic contacts on ZnO. Contacts are made by depositing metal on the surface creating a junction. A good Ohmic contact lets the current pass both for reverse and forward bias, with negligible voltage drop, and are relatively easy to make with aluminium or titanium on n-type ZnO [5].

In this chapter we will go through the basic theory behind the Schottky contacts. The reader is referred to e.g. Refs. [9, 46, 47] for a more detailed review.

8.1 Schottky diode theory

Unlike Ohmic contacts, a Schottky diode has rectifying ability; In the ideal case, it lets the current pass only in one direction. This unilateral behaviour in not unlike a p-n junction, but in contrast the Schottky diode is a majority carrier device. Today Schottky contacts on n-type ZnO are difficult to make. Among other things, they

suffer from low barrier height and high series resistance. This can, for instance, be due to native surface defect states [48] and/or an electrically conductive layer on the surface of ZnO [49]. Here we will be presenting Schottky theory for a n-type semiconductor, but the same theory is true for p-type semiconductors (and holes).

When a metal with a work function[1] ϕ_m bigger than the semiconductor's ϕ_{sc}, is brought into contact with a n-type semiconductor (n-SC), electrons from the n-SC will diffuse over to the metal, leaving behind uncompensated ionized dopants. These positively charged dopants and the image charge collected on the metal are called *the diffusion layer W*, and set up an internal electrical field $\vec{E}_i$ which inhibits further diffusion. This layer is assumed to be depleted of carriers while the outside remains neutral, and that it is abrupt and well defined; Collectively it is called *the depletion approximation*.

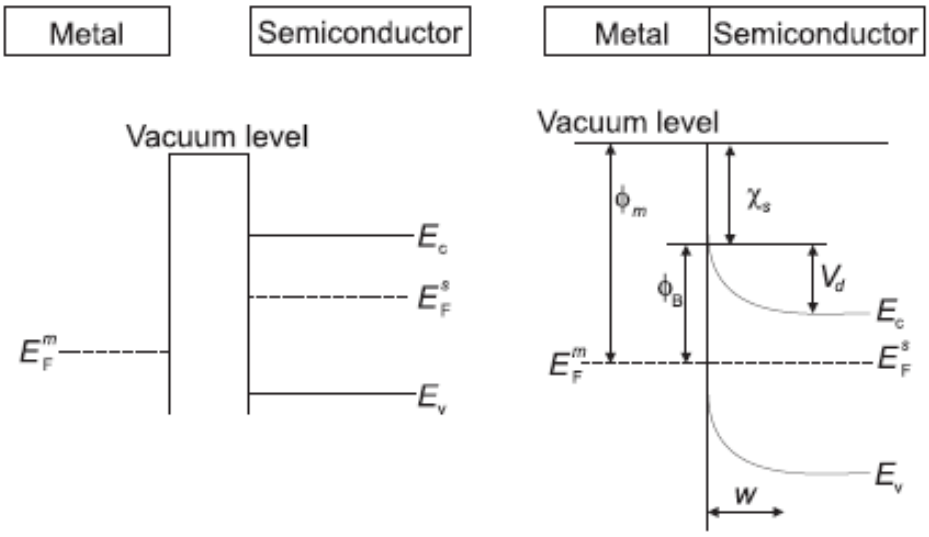

Figure 8.1: Band-gap overview of a Schottky contact. Left: Band-gap structure before putting the metal and SC in contact. Right: In contact and at equilibrium. Figure adapted from Ref. [2].

Before metal and n-SC are in contact, the Fermi level of the semiconductor is higher (figure 8.1). In equilibrium they align by raising the electrostatic potential

[1] Work function is defined as the amount of energy needed to excite one electron from the Fermi level to vacuum level (figure 8.1).

of the semiconductor (lowering the electron energy with respect to the metal). The resulting band bending (at equilibrium) is governed by the following three condition [50]:

- The Fermi levels of the semiconductor and the metal must be constant throughout the system.
- The electron affinity[2] must be constant.
- The vacuum level must be continuous.

This band bending introduces a barrier ϕ_b for the electrons, also known as *the Schottky barrier*. Ideally (from Schottky-Mott theory), this barrier is unaffected by an external bias V and given as

$$\phi_b = \phi_m - \chi_{sc} \tag{8.1}$$

In order for an electron to diffuse to the metal at equilibrium, it has to surpass a contact potential V_d. This potential barrier can be manipulated as $V_d - V$ by applying a bias V (and thus will no longer be in equilibrium). A forward (positive) bias reduces the potential barrier making it easier for the electrons to diffuse over to the metal, and thus reducing the depletion width W. A reverse (negative) bias increases the barrier, making the current flow from the SC to the metal negligible by increasing W.

8.1.1 Thermionic emission theory

At non-equilibrium state, electrons are able to cross the depletion region by means of diffusion and drift, and then they have to go through to the metal by thermionic emission. According to *the diffusion theory* the bottle neck for the charge transfer over the depletion layer is the diffusion and the drift, not the thermionic emission rate. However, in the case of a Schottky contact with fairly high carrier mobility, as it is in our case, the impeding factor is the thermionic-emission rate and best

[2]Electron affinity χ is energy needed to excite one electron from conduction band edge to the vacuum level (figure 8.1).

described by *the thermionic emission theory*. Thus, the thermionic theory ignores the affects of diffusion and drift, and the mobility in the depletion region is assumed to be infinite.

By introducing a ideality factor η, the current density J is given by

$$J = J_0 \exp(\frac{qV}{\eta kT})(1 - \exp(-\frac{qV}{kT})) \tag{8.2}$$

where J_0 is the reverse saturation current density

$$J_0 = A^* T^2 \exp(-\frac{q\phi_b}{kT}) \tag{8.3}$$

A^* is the effective Richardson constant given in table 2.1, k is the Boltzmann's constant, q is the electron charge, V is the applied bias, and $J = I/S$ where I is the current and S is the cross-section area of the junction.

8.1.2 Capacitance of a Schottky diode

If a negative bias is applied to an ideal Schottky diode (with n-type semiconductor), the width of the depletion layer will increase as a response to the applied external field, because more uncompensated dopants are left behind. If a small AC signal with a frequency f is applied, a capacitance C will arise.

A general definition of the capacitance can be obtained from applying Gauss's theorem to a surface enclosed by two planes parallel to the junction, with one plane in the deletion layer and the other in the bulk of the SC where the bands are flat

$$C = \varepsilon_s \frac{\partial \vec{E}_i}{\partial t} = \frac{\partial Q}{\partial V} \tag{8.4}$$

where $\vec{E}_i$ is the internal field. In the case of negligible minority carriers and by assuming the depletion approximation, the charge Q can be given as

$$Q = \varepsilon_s E_{i,max} = S\sqrt{2q\varepsilon_s N_d \left(V_d - \frac{kT}{q}\right)} \tag{8.5}$$

where N_d is the donor concentration, ε_s is the ZnO's permittivity given in table 2.1 and V_d is the equilibrium contact potential. Combining equations (8.4) and (8.5)

gives the capacitance as

$$C = \left| \frac{\partial Q}{\partial V} \right| = \frac{S}{2} \sqrt{\frac{2q\varepsilon_s N_d}{V_d - V - \frac{kT}{q}}} \tag{8.6}$$

where V is the applied bias.

8.2 Deviations from ideal Schottky diodes

Here we will present some of the deviations that are often seen in real Schottky contacts opposed to the simple theory presented above.

The theory assumed that the Schottky barrier height was constant under applied bias. In fact, ϕ_b is a decreasing function of the electrical field, and since E_i increases with increasing reverse bias, it follows that ϕ_b decreases with increasing reverse bias. This effect is called *the image force lowering*, and arises because the conduction electrons experience a attractive force from their image charges in the metal. However, the effect is usually not observed as carrier generation and carrier tunnelling dominate reverse leakage currents [50].

In real Schottky diodes there is usually a series resistance R_s at forward bias that limits the current. An aim in diode manufacturing is to minimize R_s as much as possible. A diode with a series resistance is approximately circuit-equivalent to a capacitor in parallel with a leakage resistance R_l and in series with R_s (see figure 8.2). We will see in section 10.1 how R_s and R_l can be calculated from current voltage measurements.

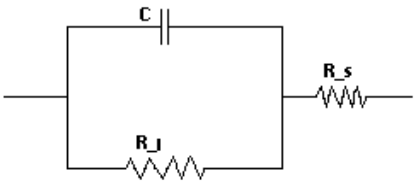

Figure 8.2: Approximated circuit equivalent to a real Schottky contact.

One way for the electrons to cross the potential barrier is via tunnelling. In moderately doped materials, even a moderately large reverse bias can cause the potential barrier to be thin enough for significant electron tunnelling from the metal to the semiconductor. This can result in "soft" IV at reverse bias (e.g. high η). In highly doped materials, tunnelling can result in a so-called *Zener Breakdown*. Tunnelling is particularly important at the edge of a contact, where the field is stronger subsequently exaggerating the image force lowering. Therefore, the current density is enhanced at the edge of the contact, and lower in the middle [50].

In addition, there can be contaminations, sputtering induced damage, undesired chemical compounds, native defects, and other factors that introduce undesired surface states. These surface states can be difficult to characterize and are probably the main cause for non-ideal Schottky behaviour [50].

9 Experimental procedure and previous work

Research is the process of going up alleys to see if they are blind.

– Marston Bates

9.1 Schottky diode deposition procedure

In this experiment we minimized the Li concentration and the resistivity in 1x1cm^2 ZnO samples by annealing. As observed in part one, sample annealed at 1600°C had the lowest Li bulk level and resistivity. However, since the sample did not withstand such a high temperature and started to evaporate, we performed the annealing at 1500°C. They were then polished and divided into smaller pieces (figure 9.1), before depositing circular 100nm thick palladium (Pd) contacts by electron beam evaporation with three different diameter sizes using a shadow mask: 260$\pm$10μm, 460$\pm$10μm and 750$\pm$10μm.

The polish was done since the 1500°C anneal made the surfaces rough and not adequate for contact manufacturing, as shown in figure 6.3. The resistivity after polishing was the same as before, $\approx 0.5\Omega$cm. The samples were cleaned before deposition: total of three times in five minutes of acetone, ethanol and hydroperoxide. After deposition they were annealed for 1/2h at 200°C. The 200°C post-anneal and cleaning in hydroperoxide was done for improving the contacts as reported by

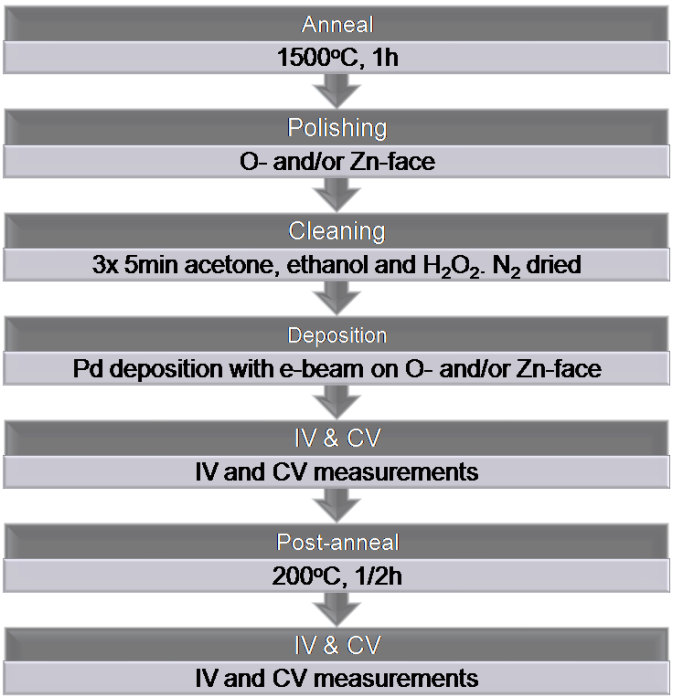

Figure 9.1: Overview of the experimental procedure.

Schifano et al. [51]. The contacts were deposited on both faces to reveal any polarity effect. Backside contacts were made by covering the side with eutectic InGa. They were remeasured after 15days for stability check.

9.2 Polishing

The samples were glued to a metal holder with the side to be polished on top. It was then gently pushed towards a rotating disc covered with diamond-dust slurry. Diamond sizes ranged from rough 15µm to very fine 1/2μm. The samples were taken through the different diamond sizes in order to smoothen the surface topography. They were inspected with an optical microscope many times during polish to control the progress. Finished samples were generally smooth and shiny except for some few deep craters, as mentioned in section 6.2. However, this procedure was inaccurate and depended solely on the experience (and gut-feeling) of the user,

resulting in a somewhat varying outcome.

9.3 Electron beam evaporation

Electron beam evaporation (e-beam) is a deposition technique, in which a crucible containing the material to be evaporated is heated up until a sufficient rate of evaporation is established. The samples have to be carefully positioned so they face downward and are rotated for the most uniform deposition. A tungsten (W) filament is typically used to emit the electrons, which are in turn bended by a strong magnetic field so they incident on the source and heat it up (see figure 9.2). Usually the beam is rastered to heat a bigger portion. Heating up this way minimizes contamination from the crucible.

The deposition was done at $\approx 10^{-6}$mbar pressure with a 99.999% pure Pd source and a molybdenum mask.

9.4 Previous experimental work

Reproducible, high quality Schottky diodes are difficult to make, which is reflected in the *few* reported results for high quality diodes. Table 9.1 gives an overview of some of the work that has been reported. The best results with Pd are from samples which have been cleaned with organic solvent and hydrogen peroxide [51], giving a current rectification from -2V to 2V of up to 8 orders of magnitude. Grossner et al. [52] have reported low ideality factor of 1.03 and barrier height of 0.83eV with Pd contacts after organic solvent clean only. Other metals like silver (Ag) and gold (Au) have also given high Schottky barriers of 0.6-0.8eV with n-ZnO [5].

Schottky fabrication on ZnO seems to be a case of “hit-and-miss”; Some few contacts in a batch show much stronger rectification, indicating a strong influence from surface states [2].

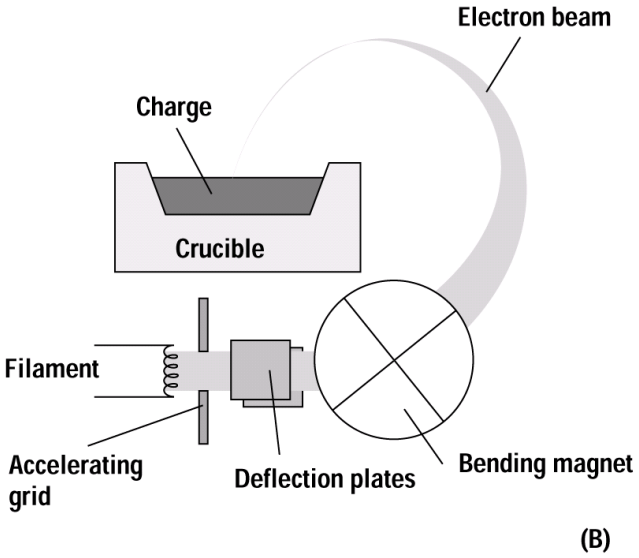

Figure 9.2: Schematic overview of a electron beam heating system. The electrons are emitted from a filament, typically Tungsten, then bended into the crucible to heat the material to be evaporated. Figure adapted from [13].

Contact metal	Deposited on	Surface treatment	η [eV]	ϕ_b	Ref.
Au/Pt	Zn	Ozone clean	1.5	0.7	[53]
Pd	O	Organic clean	1.03	0.66	[52]
Pd	Both	dimethylsulfoxide	1.75	0.73	[54]
Pt	O	Boiling $(NH_4)_2S_x$	1.51	0.79	[55]
Pd	O	hydroperoxide	≈ 1	$\approx 1.0-1.2$	[51]

Table 9.1: Overview of some of the reported Schottky diodes manufactured on ZnO [2].

10

Electrical characterization techniques

If the facts don't fit the theory, change the facts.

– Albert Einstein

The current-voltage (IV) and capacitance-voltage (CV) measurements were done from -2V to 2V in a dark chamber at RT with Labview connected by GPIB to either *Keithley 6487* or *HP Agilent 4284A*, respectively. We will here present the analysis methods for the data collected.

This chapter is based on theory from Refs. [46, 47].

10.1 Current-voltage measurements

As figure 8.2 shows, we need to take into account the voltage drop resulting from the series resistance R_s. This is done by replacing the applied bias V with $V_{eff} = V - I \times R_s$. If $V > 3kT/q$ and $I = J \times S$, eq.(8.2) can be written as

$$I \approx I_0 S \exp(\frac{qV_{eff}}{\eta kT}) \tag{10.1}$$

By taking the derivative of eq.(10.1) with respect to V, one obtains

$$\begin{aligned} \frac{1}{I}\frac{\partial I}{\partial V} &= \frac{q}{\eta kT} - \frac{q}{\eta kT} R_s \frac{\partial I}{\partial V} \\ &= a - b\frac{\partial I}{\partial V} \end{aligned} \tag{10.2}$$

At higher values of V (typical from $\geq$ 1V) the series resistance dominates. By plotting $\frac{1}{I}\frac{\partial I}{\partial V}$ vs $\frac{\partial I}{\partial V}$ at these values one gets a straight line with slope $b = \frac{q}{\eta kT}R_s$, so that $R_s = \frac{a}{b}$.

The ideality factor η must be estimated from eq.(8.2), because eq.(10.1) is only valid for $V > 3kT/q$. By rearranging eq.(8.2) and derivating with respect to V, $1/\eta$ is given by

$$\begin{aligned} J_0 \exp\frac{qV}{\eta kT} &= \frac{J}{1-\exp(-\frac{-qV}{kT})} \\ \frac{1}{\eta} &= \frac{kT}{q}\frac{\partial}{\partial V}\ln\Big(\frac{J}{1-\exp(-\frac{qV}{kT})}\Big) \end{aligned} \tag{10.3}$$

10.2 Capacitance-voltage measurements

As mentioned in section 8.2, measurements on real Schottky diodes are affected by both the R_s and R_l. This means that the measured capacitance is not the same as the actual capacitance over the diode. This can be accounted for by a correction factor

$$\frac{C_m}{C} = \Big((1+\frac{R_s}{R_l})^2 + (\omega C R_s)^2\Big)^{-1} \tag{10.4}$$

where C_m is the measured capacitance, C is the actual capacitance over the diode, $\omega = 2\pi f$ is the angular frequency and f is the probing frequency. Accurate measurements require the criteria $R_s \ll R_l$ and $R_s \ll (\omega C)^{-1}$, so that the capacitor is the dominant circuit element. R_s is calculated from the IV as shown in section 10.1 and R_l can be calculated from the conductance σ as

$$\sigma = \frac{1}{R_l(1+(\omega C R_s)^2)} \tag{10.5}$$

A plot of $\frac{1}{C^2}$ from eq.(8.6) against bias when criteria $R_s \ll R_l$ and $R_s \ll (\omega C)^{-1}$ are fulfilled *and* no appreciable interfacial layer exists, should give a straight line

$$\begin{aligned} \frac{1}{C^2} &= (\frac{2}{S^2 q N_d \varepsilon_s})(\phi_b - \xi - V - \frac{kT}{q}) \\ &= (\frac{2}{S^2 q N_d \varepsilon_s})(\phi_b - \xi - \frac{kT}{q}) - (\frac{2}{S^2 q N_d \varepsilon_s})V \\ &= c - gV \end{aligned} \tag{10.6}$$

Here c and g are constant and V_d is replaced by $\phi_b - \xi$, where $\xi \approx 0.1$eV is the difference between the Fermi level and the bottom of the conduction band for a 1500°C annealed sample calculated in section 6.2. The line in eq.(10.6) will intercept at $V_I = \frac{c}{g}$ when extrapolated to $1/C^2 = 0$, which in turn gives the barrier height as

$$\phi_b = V_I + \xi + \frac{kT}{q} \tag{10.7}$$

The crucial step is to know when the criteria are no longer valid, and thus C_m over this point can not be used in calculations of ϕ_b or the effective donor concentration N_d (shown below). If R_s is small, the criteria are valid also for very small forward bias, making the calculation of ϕ_b more accurate.

To a first approximation the capacitance in a Schottky diode can be described as a capacitance in a ideal parallel plate capacitor with the neutral regions as the plates and the depletion layer as dielectric

$$C = \frac{\varepsilon_s S}{W} \tag{10.8}$$

where W is the width of the depletion layer[1]. The effective donor density N_d, when the criteria are met, can be given as

$$\frac{1}{N_d} = -\frac{\varepsilon\varepsilon_0 S^2 q}{C^3}\left[\frac{\partial C}{\partial V}\right] \tag{10.9}$$

Now N_d and W from equations (10.9) and (10.8) respectively, can be plotted for the same C-values to get a carrier concentration profile close to the surface. Probing at low frequencies has an advantage over higher frequencies, in that they can give N_d closer to the interface, because the criterion $R_s \ll (\omega C)^{-1}$ is valid for higher forward bias.

The capacitance is affected by the energy position of the dopant levels; The deeper the levels, the lower the emission rate, and thus less contribution to the total capacitance measured at higher probing frequencies. This fact can be exploited by probing with different frequencies in order to get a picture of the dopant levels. We used six different frequencies: 1Mhz, 250kHz, 60kHz, 16kHz, 4kHz and 1kHz.

[1] The actual width of the depletion layer is $W = x_p + x_n$, where x_p is the extent into the metal and x_n in the semiconductor, but in a Schottky x_P can be neglected and $W \approx x_n$.

11 Results

The important thing in science is not so much to obtain new facts as to discover new ways of thinking about them.

– Sir William Bragg

In this chapter we will present the various preparation methods explored for Schottky manufacturing, and the results obtained from the electrical measurements.

11.1 Schottky contact deposition

100nm thick circular Pd contacts were deposited with e-beam evaporation on ZnO samples. All the samples were annealed at 1500°C, but both the polishing and deposition were varied from just O- or Zn-face, to both. If nothing is specified, both sides are polished. After deposition IV and CV were measured, and then they were annealed for 1/2h at 200°C in air, before remeasuring IV and CV. This annealing step is reported to decrease the reverse current [51]. The current density rectification (or just rectification) is the difference in current density at $V = -2$V to $V = 2$V (or until the Kiethly instrument reached its current compliance of 20mA).

We did not observe any difference in IV or CV characteristics depending on the contact size, therefore we will not discriminate between them and state the current densities instead of current. For typical IV and CV characteristics for the different contact types presented below, see appendix B.

11.1.1 Contact deposition on Zn-face

First we deposited on the Zn-face of an unpolished sample; The rough O-face worked as the back contact. This did not yield any good rectifying or ohmic contacts, and on average only worked in the interval $V \in [-0.3V, 0.3V]$. Depositing on the Zn-face with a polished O-face did not improve the results, neither did 200°C post-anneal.

What was more surprising was that when both sides were polished, contacts on Zn-face showed good *Ohmic* behaviour. The reverse current decreased with the 200°C post-anneal, but only slightly (figure 11.1), giving minor rectification.

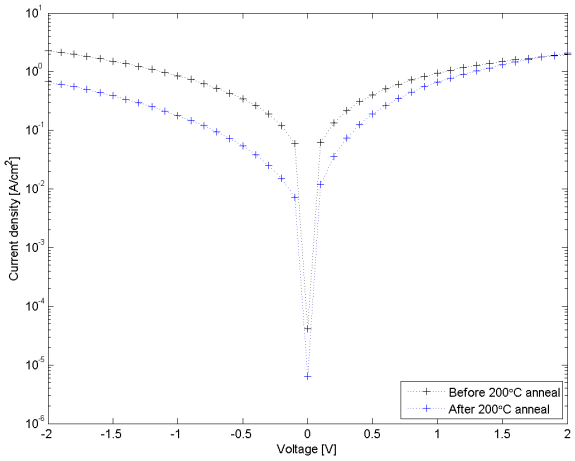

Figure 11.1: IV before and after 1/2h 200°C post-anneal of a contact on the Zn-face. Voltage applied from reverse to forward direction.

11.1.2 Contact deposition on O-face

As seen in figure 6.3, the O-face at 1500°C was very rough. So the notion of depositing on an unpolished O-face was discarded early on. Contacts made on polished the O-face, with the unpolished Zn-face as back contact yielded good Schottky contacts with typical rectification in the range of three to four orders of magnitude. 200°C post-anneal improved the contacts slightly (figure 11.2).

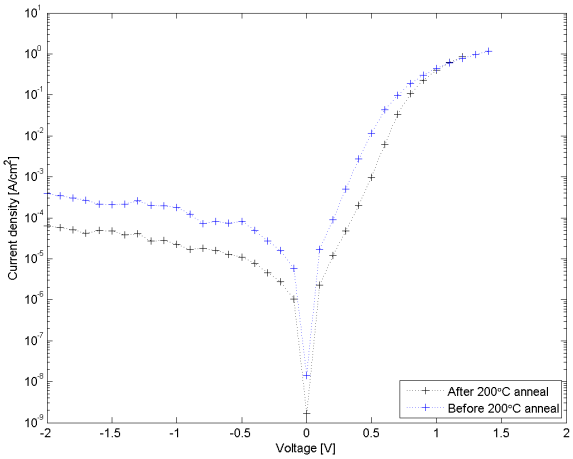

Figure 11.2: IV before and after 1/2h 200°C anneal of contact deposited on O-face with unpolished Zn-face back contact. Voltage applied from reverse to forward direction.

The best Schottky contacts were achieved when samples were polished on both sides, deposited on the O-face, and then annealed at 200°C for 1/2h in air. This gave a typical rectification in the range of four to six orders of magnitude, while a few very good ones, were between 7 to 8 orders of magnitude. Figure 11.4 shows a contact with rectification of eight orders and comparing the red and the black curve reveals the effects of annealing.

11.1.3 Contact reproducibility

The reproducibility of the contacts was somewhat of a challenge. Typically, two-third of the contacts on a sample showed similar behaviour, a few excelled, while the rest showed low to no rectification. As mentioned in section 6.3, big pits were created on the surface after the 1500°C-anneal, which were difficult to remove. The samples were therefore cut in smaller parts in a way to avoid pits on one part, and rather have them all on the other. This resulted in a improved rectification of up to two orders of magnitude compared to the sample with pits.

11.1.4 Contact stability

There was a difference in which way the bias was applied during the measurements, and this difference was apparent in most of the contacts. Bias applied from positive to negative direction (PN) usually gave a more stable reverse current, while negative to positive (NP) gave a decease in reverse current when approaching zero voltage (figure 11.3). However, as we will show below, consecutive measurements showed better rectification with PN than NP[1].

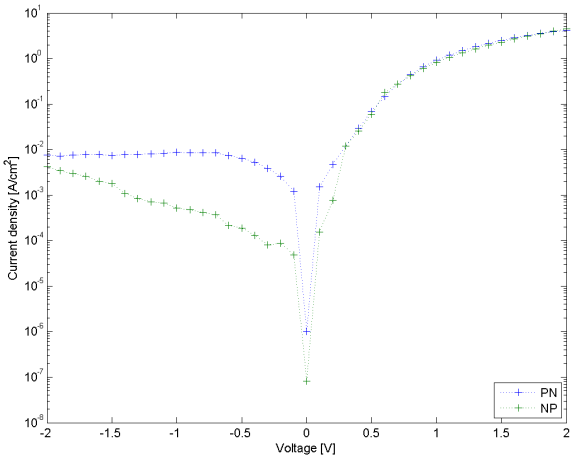

Figure 11.3: IV of a contact made on O-face. The data show the decrease in reverse current density if the bias is applied from reverse to forward direction.

Typically, the very first run showed the lowest reverse current, and after two-three consecutive NP sweeps the reverse current increased, and thus resulted in less rectification. This initial degrading could be of up to four orders of magnitude. Comparison of the blue and the red curve in figure 11.4 shows the degrading effect of consecutive measurements. Further observations revealed that PN worked in the opposite manner; It gradually recovered the negative impact of NP till *some* extent (figure 11.5). There seemed to be two stable reverse current levels; One for NP and

[1] We will indiscriminately refer to both NP/PN bias paths and forward/reverse bias as bias directions, but the appropriate meaning should be clear from the context.

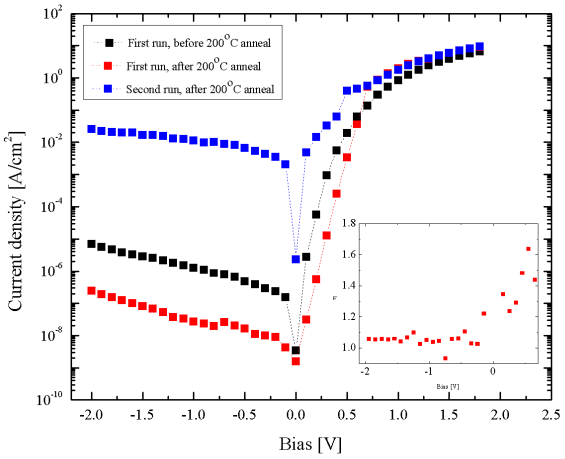

Figure 11.4: Schottky contact on the O-face with rectification of up to eight orders of magnitude, before and after 200°C post-anneal. Also shown is the affect of consecutive NP measurement and η calculated from eq.(10.3) for the *first run, after post-anneal*.

one for PN. When the level for NP sweeps was reached, which only needed two-three sweeps, the reverse current could not be increased further. The same with PN sweeps, the current could not be decreased more than a certain level. Typically, these levels were at the most up to three decades apart. However, the contacts never recovered completely back to the IV measured at the very first measurement run. E.g. in the case of the contact in figure 11.4, PN measurements could only recover about two decades in reverse current from the *Second run, after* 200°C *anneal* (not shown here). In addition, we found out that samples stored at RT in an exsiccator for a few days with no bias applied, also had recovering effect. These effects were independent of the surface polarity.

To investigate the reason for this dependence on the voltage direction, we made an InGa ohmic contact on the front of the sample (on the same side as the Schottky contact). This did also show the same dependence on the voltage direction as with the ohmic contact on the Zn-backside

All the contacts showed a non-permanent soft breakdown (figure 11.5) with bias exceeding 4V. They also did not show any degradation over a 15day period stored in an exsiccator at RT. The bias dependent IV characteristics-effect was not observed in CV measurements.

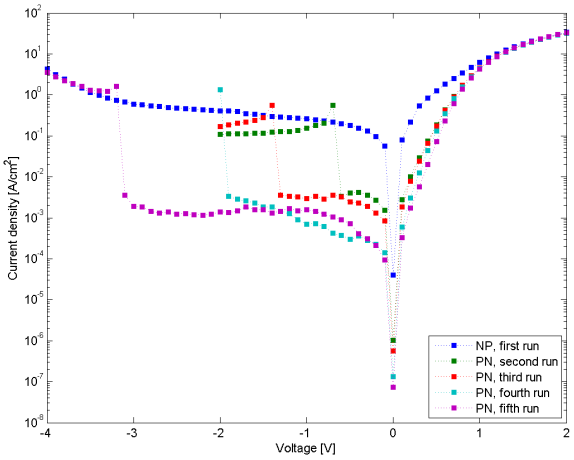

Figure 11.5: Shows the recovering effect of the reverse current with PN measurements done on a O-face contact after post-anneal. Blue curve shows soft breakdown with NP.

11.2 R_s and η from current-voltage data

The series resistance R_s was calculated from eq.(10.2), typically at $V > 1V$ (figure 11.6). R_s averaged over several contacts are listed in table 11.1. Contacts on unpolished Zn-face with unpolished O-back contact did not work, as mentioned previously, so R_s could not be calculated.

From eq.(10.3) η could be estimated as a function of bias. This gave $\eta(V < 0V) \cong 1.06$, but for forward bias it increases to $\eta(V = 0.5V) \approx 1.5$ (figure 11.4). This behaviour was typical for all the contacts.

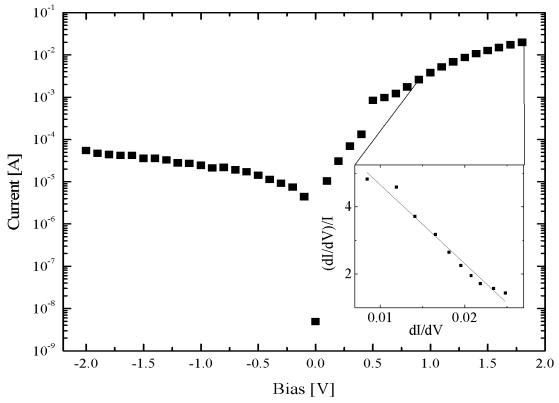

Figure 11.6: Series resistance calculated from the linear fit of eq.(10.2) for high voltage values.

Deposited on	Backside face	Average R_s [Ω]	J_r [A/cm^2]	Maximum rectification	η
Zn-face	O-face	80 ± 20	9×10^{-1}	< 0.5	1.07
O-face	Unpolished Zn	20 ± 3	3×10^{-4}	4	1.06
O-face	Zn-face	20 ± 6	2×10^{-7}	8	1.06

Table 11.1: The reverse current density J_r at -2V, the maximum orders of magnitude in current rectification from -2V to 2V, and ideality factor η averaged from -2V to 0V are all obtained from the best contacts only. The series resistance is an approximate number from averages over many contacts. The depositioned sides are all polished, and all the contacts have been post-annealed at 200°C.

11.3 Evaluation of capacitance-voltage data

Equations (10.6) and (10.9) are limited by the criteria $R_s \ll R_l$ and $R_s \ll (\omega C)^{-1}$. The criterion $R_s \ll (\omega C)^{-1}$ held true for all the contacts. E.g. for the contacts with the highest R_s ($\approx 80\Omega$ for Zn-face contacts) and for the highest $f = 1$MHz, the criterion $R_s \ll (\omega C)^{-1} \approx 2 \times 10^3$ was still satisfied. This simplified eq.(10.5) giving $\sigma \approx R_l^{-1}$. If we now set an upper limit, $R_{s,max} \equiv 0.5\% R_l$, for when we can use the equations (10.6) and (10.9); We get the correcting factor in eq.(10.4) to be less than 1% in a worse case scenario, meaning, to a very good approximation, that $C \approx C_m$.

CV measurements were done on the best contacts from samples deposited at Zn- and O-face (samples polished at both sides) at six different frequencies at RT with applied bias in the range of $V \in [-2, 2]$. We did not observe any significant difference in the capacitance with respect to the post-anneal of 200°C, but for the sake of consistency, we will only present the results from after the post-anneal.

11.3.1 Effective donor concentration

From eq.(10.9) the effective donor concentration N_d can be calculated as a function of depth. In figure 11.7 we show the calculated N_d for the three different contact-types with signal frequency of 1kHz: (1) deposited on O-face, (2) deposited on Zn-face and (3) deposited on O-face with unpolished Zn-backside. The three types show donor concentrations in the vicinity of mid-10^{16}cm^{-3} to low-10^{17}cm^{-3}.

There were two trends in N_d that persisted in most of the measurements (figure 11.8): A decrease in the concentration closer to the surface regardless off the frequency, and an offset of the donor profile, shifting closer to the surface with decreasing frequency.

11.3.2 Barrier height

Barrier height was calculated by extrapolating the linear part of $\frac{1}{C^2}$ for reverse and small forward bias (keeping in mind the criterion $R_s \ll R_l$), and using eq.(10.6) and eq.(10.7). Figure 11.9 shows a CV measurement at 1kHz and the $\frac{1}{C^2}$ as inset.

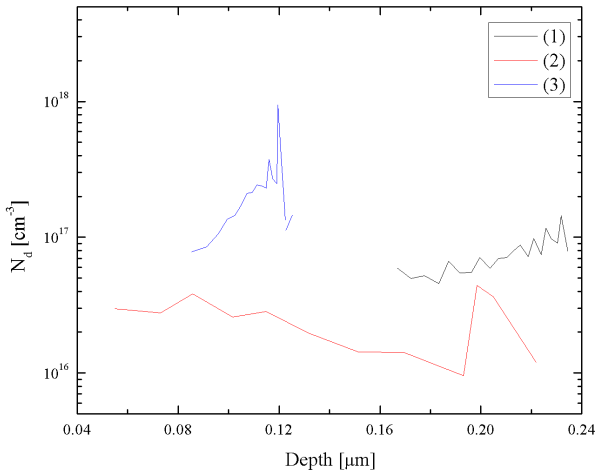

Figure 11.7: Measurements are done at 1kHz. N_d calculated from eq.(10.9) for contacts: (1) O-face, (2) Zn-face and (3) polished O-face, unpolished Zn-backside.

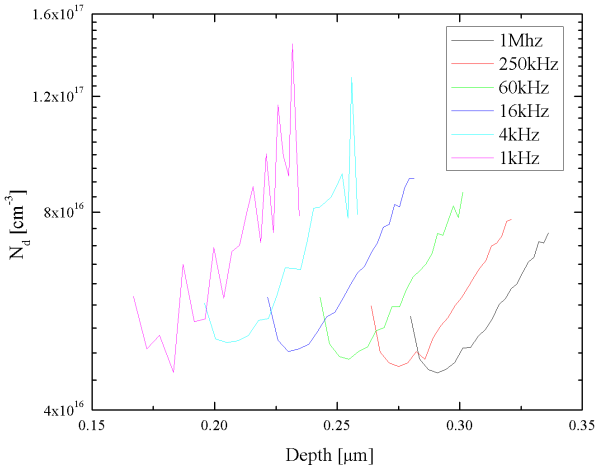

Figure 11.8: A decrease in the donor concentration close to the surface, and an increasing offset with probe frequency are clearly seen for a contact deposited on O-face.

Unfortunately, only a small handful of measurements were as good as figure 11.9. The majority of the measurements were far from ideal and gave unreasonable results for the barrier height. Of the few good measurements, we got reasonable results for ϕ_b of 0.67 ± 0.06eV and 0.57 ± 0.01eV at 1kHz signal frequency from O-face contacts.

In addition to giving non-ideal CV measurements, the contacts on Zn-face also suffered from low R_l (high conductance), and thus the criterion $R_s \ll R_l$ was never fulfilled.

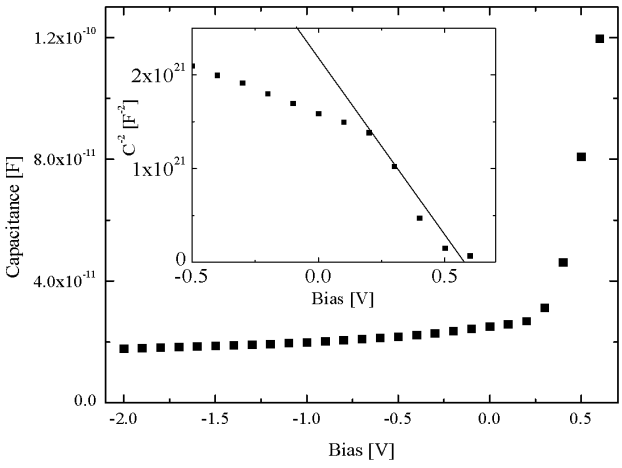

Figure 11.9: 1kHz CV-measurement up to $R_s \ll R_l$ for a contact at O-face, with both sides polished. Inset shows $\frac{1}{C^2}$ linear fit giving a $\phi_b \approx 0.67 \pm 0.06$eV.

12 Discussion

Nothing shocks me. I'm a scientist.

– Harrison Ford, Indiana Jones

12.1 Effects of the surface topography

Surface topography was crucial for the quality of the contacts. Not surprisingly, did the unpolished, rough Zn-surface prove difficult to make working contacts on. It did not matter if the backside was polished or not, as long the deposited side was rougher with a rms exceeding 50nm, the deposited contacts were of poor quality.

At 1500°C the depth of the pits increased, as mentioned in section 6.3. These were difficult to fully polish away, and we also found out that they had negative effect on the Schottky contacts. One sample was cut into two pieces; one with pits, the other one without. The one without the pits had a rectification of up to two orders of magnitude better than the one with pits. Since it was the same sample, there was no difference in the preparation. Therefore we can conclude that a deep pit, with an estimated depth of $> 60\mu$m, degrades the contacts in a much larger area than the actual size of the pit itself, suggesting substantial extension of defects outside the pit area observed optically.

12.2 Effects of the lithium concentration

We found the lithium concentration on the backside, independent on the polarity, to be very crucial for the quality of the contacts. As shown in part one, the Li concentration accumulated at the surface as the annealing temperatures were increased. The accumulation at the backside did not have to be more than a few microns before having a very degrading effect on the rectification. Samples with polished Zn-backside compared to unpolished ones, showed up to four decades better rectification (figures 11.2 and 11.4). Samples with unpolished O-backside, did not work, while polished backside showed a öhmic/minor rectifying behaviour (figure 11.1). This could be due to smoother backside surface, but we believe the main cause is the removal of the accumulated Li concentration (cf. figure 7.1), and thus removing a high concentration of Li_{Zn}-acceptors.

Li dependence on contact quality could also explain why a few of the contacts on all the samples malfunctioned completely. These contacts may have been deposited right on top of the Li-dense areas shown in figure 7.3.

12.3 Effective donor concentration

The behaviour of the decreasing concentration towards the surface as seen in figure 11.8, has been reported by other authors as well [51, 56, 57]. It has been suggested that a defective layer of Zn vacancies or vacancy clusters acting as compensating centres, is formed close to the surface by the H_2O_2 treatment.

The observed offset in N_d (figure 11.8) indicates existence of deep states, because the deeper states have lower emission rate and therefore cannot respond to higher probe frequencies; They "freeze" out. This is in agreement with findings of Pearton et al. [5] which showed high concentration of deep states at 0.55eV and 0.65eV introduced by the mechanical polish. They also suggested a 9-10min HNO_3 etch to remove these states.

12.4 Interfacial layer

There are numerous indications that are pointing in the direction of an interfacial layer existing between the Pd contacts and the ZnO substrate, independent of the O- or Zn-face. First, there is the ideality factor η. It is close to one for reverse bias, indicating thermionic emission as a major mechanism for current transport, and then deviating very much for forward bias. Such a deviation is suggested by Rhoderick et al. [46] to be due to thick interfacial layer.

Good CV measurements were difficult to obtain, because, as shown in figure 11.8, N_d was a function of depth while in our calculations we assumed a constant N_d (eq.(10.9)). The few good measurements we did manage to obtain could a result of very thin/no interfacial layer, thus indicating a non-uniform layer. Barrier heights calculated from these few good contacts were $\approx 0.67 \pm 0.06$eV and 0.57 ± 0.01eV.

An ohmic InGa contact on the front was made to investigate the charging effect. However, we were not able to make the contact directly on the substrate. The contact worked after the O-surface had been scratched with a diamond pen. This supports the existence of an interfacial layer. In addition, it revealed that the layer probably is highly resistive on the O-face and only few microns thick. This layer is not possible to measure with standard four point probe measurement, since the probes easily penetrate more than few microns when measuring.

The origin of the interfacial layer could be the mechanical polish and the hydroperoxide clean. Our samples were cleaned five minutes in H_2O_2, which is thought to remove many of the deep states introduced by Zn interstitials and O vacancies, but it is also believed to introduce some of its own compensating vacancy clusters and zinc vacancies [51]. Mechanical polish is believed to introduce deep states [5], but as mentioned previously, a 9-10min etch in concentrated HNO_3 could remove them.

12.5 Charging effect

The IV-characteristics for nearly all the contacts, independent of the surface polarity, were dependent on the sign of the voltage gradient, as shown in figure 11.5.

We believe this is caused by a charge to build up at the surface and could be eliminated by passivating the contacts. This can be done with photoresist (figure 12.1) or more rigorously by making a guard ring [46]. Our hypothesis is that a better passivation will prevent the bias direction dependent behaviour, and may also reduce the leaking edge current, thus reducing the reverse current.

Figure 12.1: A possible way to examine the charging effect is to isolate the Pd contacts with photoresist.

Part III

Conclusion and suggestions for future work

13 Summary

The important thing is not to stop questioning.

– Albert Einstein

13.1 Conclusion

In the first part of this thesis, we investigated the affects on the high, constant Li concentration of 10^{17}cm^{-3} present in HT grown ZnO by high temperature annealing, and subsequently how the electrical resistivity and surface topography were affected. Annealing was done isochronally for 1h at each temperature up to three times, 300°C apart, on a single sample. This revealed that the Li concentration was unchanged up to 900°C-anneal, after which the concentration decreased gradually down to 10^{13}cm^{-3}, 5μm from the O-face, at 1600°C. It also revealed that from 1100°C and upwards, Li accumulated close to the surface. The accumulation on O-face was much deeper than first anticipated for high temperatures, while on Zn-terminated face the accumulated profile was no more than a several microns deep. For comparison, at 1500°C the actual Li bulk level of 10^{13}cm^{-3} was observed after polishing the O-face to a few tens of μm, while at the Zn-face the concentration decreased to 10^{13}cm^{-3} after no more than 2μm. We argued that this would mean a Li diffusion barrier at both faces, but because of the spontaneous polarization and plausibly higher Li traps at O-face, a deeper accumulation is seen at the O-face.

We believe that the Li_{Zn}-acceptor levels play a vital role in reducing the resistivity of HT ZnO. Our experiments show a direct correlation between the Li concentration and the resistivity when annealed above 800°C; Both were reduced with four orders of magnitude after annealing at 1500-1600°C. This could be explained as a reduction in the compensating Li_{Zn} acceptor levels. A sharp increase in resistivity was observed at 600°C, while the Li concentration remained stable. As Keisser et al. [45], we too believe that this behaviour is primarily due to Li_{Zn}-H; At 600°C Li_{Zn}-H centres are broken up and H diffuses out. This increases the number of compensating acceptors, thereby reducing the conductivity.

Not surprisingly, did the sample topography change with annealing temperature. What was surprising though, was the distinct difference between the O-face at 1300°C- and 1400°C-anneal – small dents turned into big pits. We also found that the O-face was much rougher than the Zn-face at annealing temperatures above 1000°C. High temperature anneal of samples with low Li concentration could reveal Li's role in the creation of pits.

We were able to make Schottky contacts with rectification of up to eight orders of magnitude, low series resistance (20Ω) and low ideality factor (1.06). The best contacts were made by annealing at 1500°C for 1h, then polishing both sides of the sample to remove any gradient in the Li profile and to smoothen the surface. They were then cut so that at least one piece did not have any pits, and then cleaned three times in acetone, ethanol and hydroperoxide, before depositing Pd contacts with e-beam. Finally, they were annealed at 200°C for 1/2h for further improvements.

Measurements on the contacts revealed, what we believe, is a charging effect and an interfacial layer. The charging effect resulted in reverse current being dependent of the direction of bias sweep. Evidence for an interfacial layer was found from CV measurements and the manufacturing procedure of InGa front contacts. The polish was believed to introduce deep states which could be the cause of the interfacial layer.

13.2 Future directions

Here we summarize suggestions of new experiments believed to further enhance the program in mastering HT grown ZnO samples.

Li diffusivity could be mapped by annealing a Li implanted sample with low background concentrations (by means of 1500°C-anneal and polish). This will shed light on which face has the higher Li diffusivity, and maybe also on the creation of the pits on O-face.

Another idea would be to grow a layer on top of the O-face with relatively high lattice mismatch with w-ZnO, and then anneal at 1000°C or higher. The lattice mismatch could facilitate small impurities like Li to diffuse out more easily and maybe preventing an accumulation. This could also make the polishing easier by not having big pits to remove, and with less polish, there would be less surface states and higher uniformity. It would also be interesting to to see if a 9-10min HNO_3 etch after the polish would improve the contacts, or maybe the polish can be replaced by an etching step in e.g. HCl. In-situ deposition of the contacts after cleaning, could help us to understand the interfacial layer more thoroughly

In addition, mapping of the energy levels in a sample with Pd contacts deposited with our recipe and a better estimate of the carrier concentration, would be of great interest. Admittance spectrometry would be ideal for this task. This could determine if Li_{Zn} is as important as we claim. Also, Hall measurements would be highly beneficial.

Isolating the Pd contacts and passivating the surface could be a way to eliminate the charging effect. Finally, it would be an idea to investigate other metals like silver and gold.

Part IV

Appendices

A

Lithium depth profiles

Here we present the Li depth profiles of all the samples.

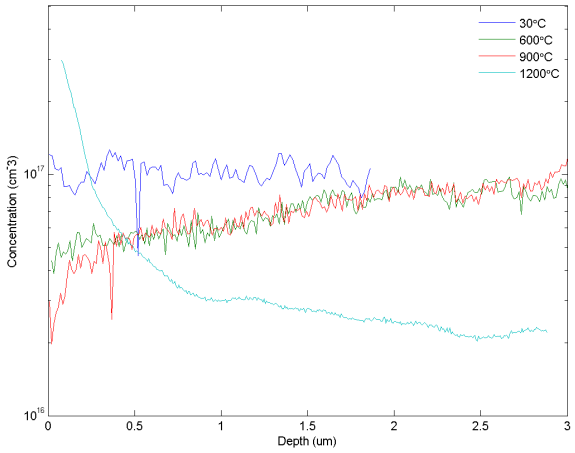

Figure A.1: Lithium profiles of sample 1 on the O-face.

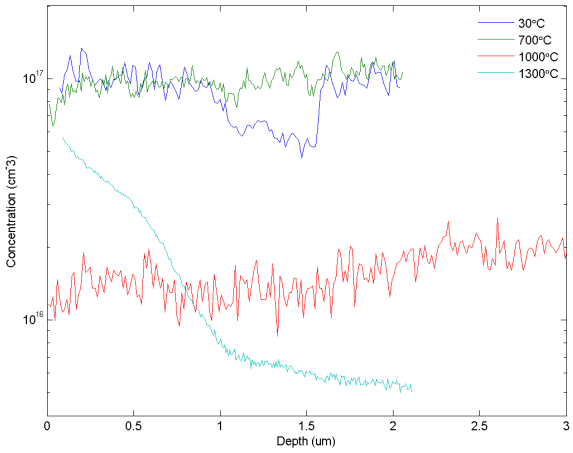

Figure A.2: Lithium profiles of sample 2 on the O-face.

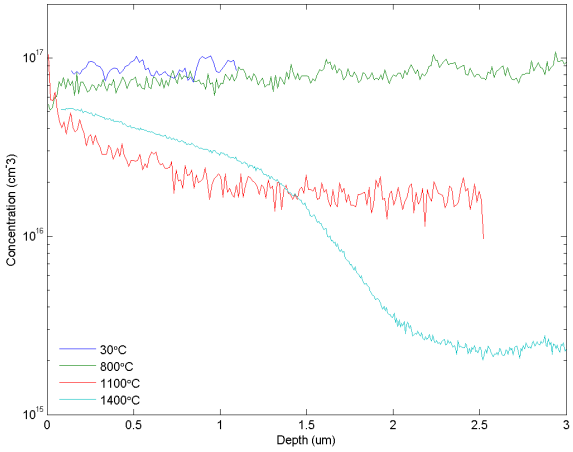

Figure A.3: Lithium profiles of sample 3 on the O-face.

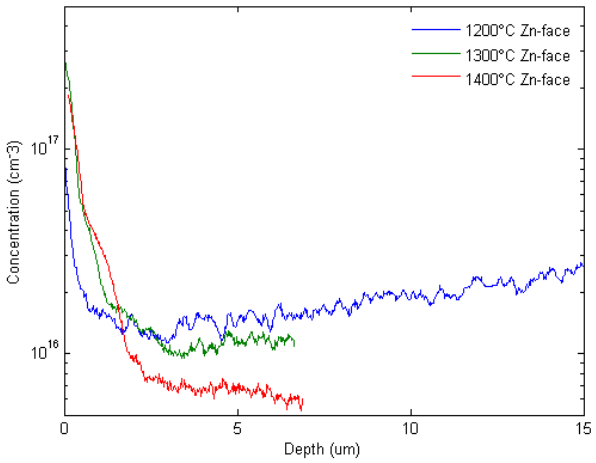

Figure A.4: Lithium profiles at 1200°C , 1300°C and 1400°C on the Zn-face.

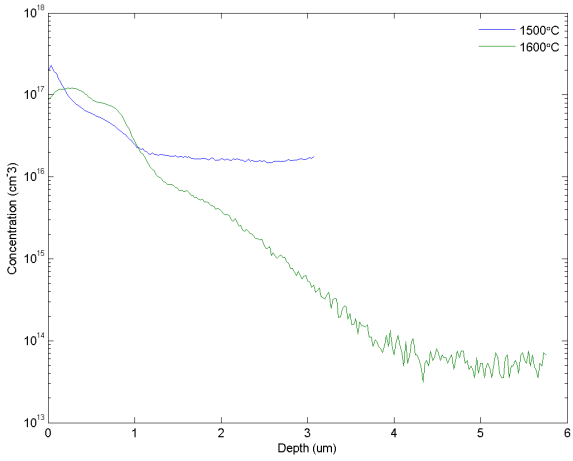

Figure A.5: Lithium profiles at 1500°C and 1600°C on the O-face.

B

Typical IV and CV results

Here we show some representative CV and IV results obtained for the different contact types. All samples have been anneal at 1500°C, and if not specified, also post-annealed at 200°C.

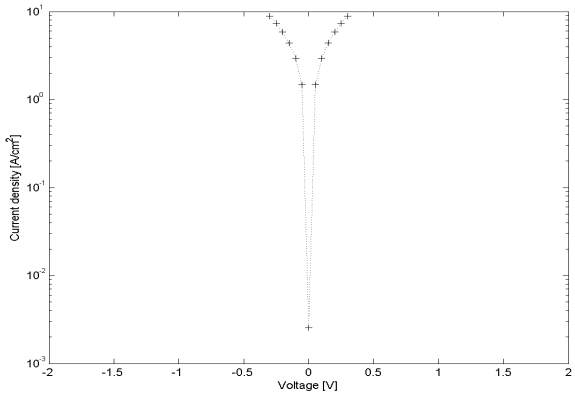

Figure B.1: Deposited on the Zn-face, neither of the sides polished.

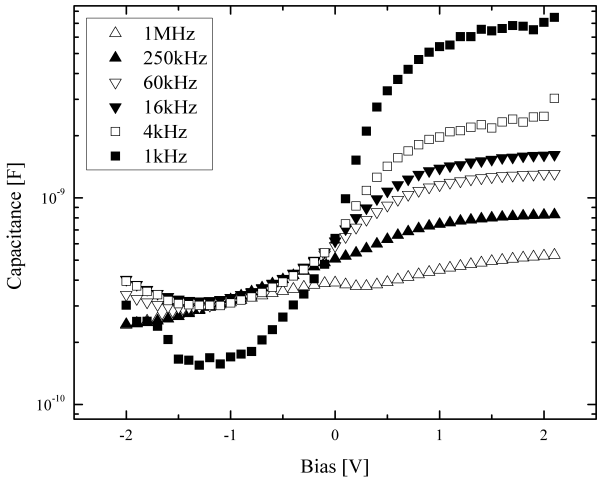

Figure B.2: The contact deposited on the Zn-face, both sides polished.

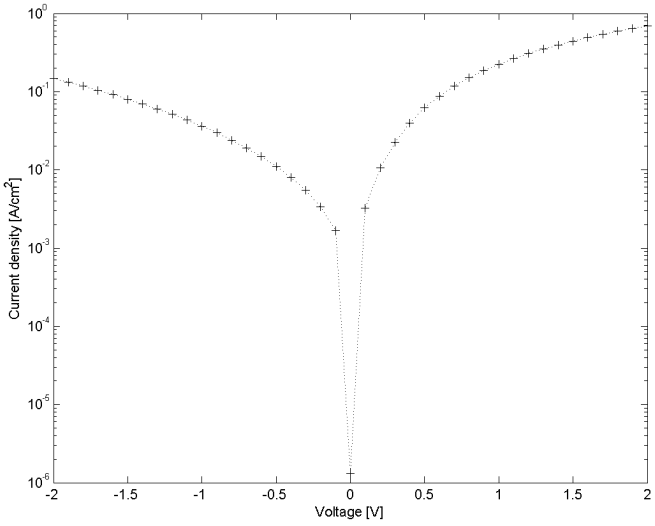

Figure B.3: The contact deposited on the Zn-face, both sides polished.

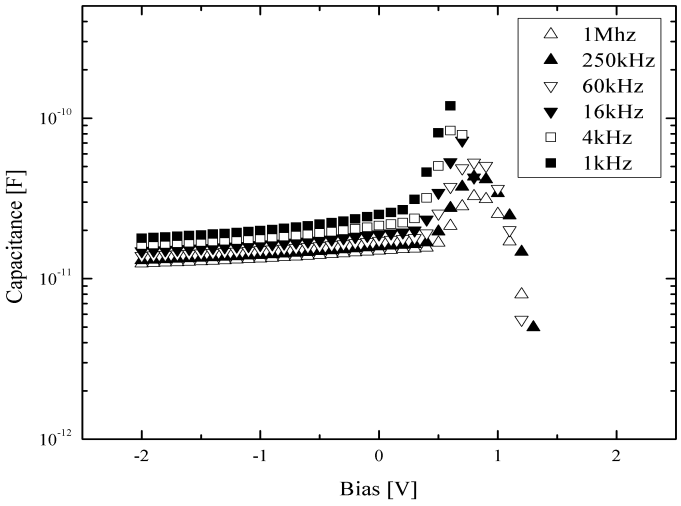

Figure B.4: The contact deposited on the O-face, both sides polished.

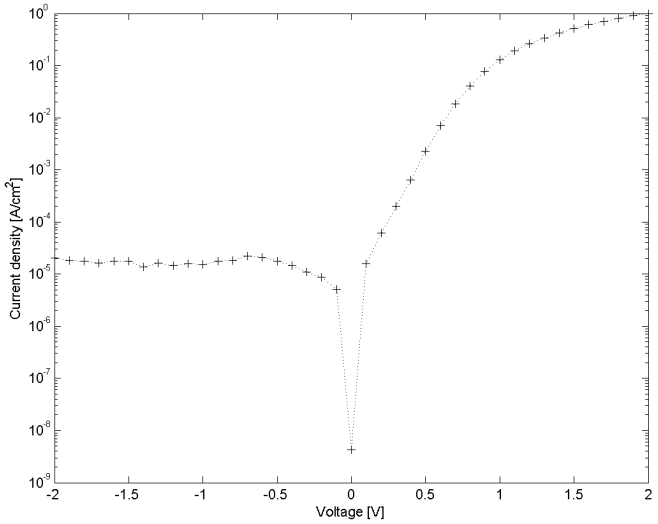

Figure B.5: The contact deposited on the O-face, both sides polished.

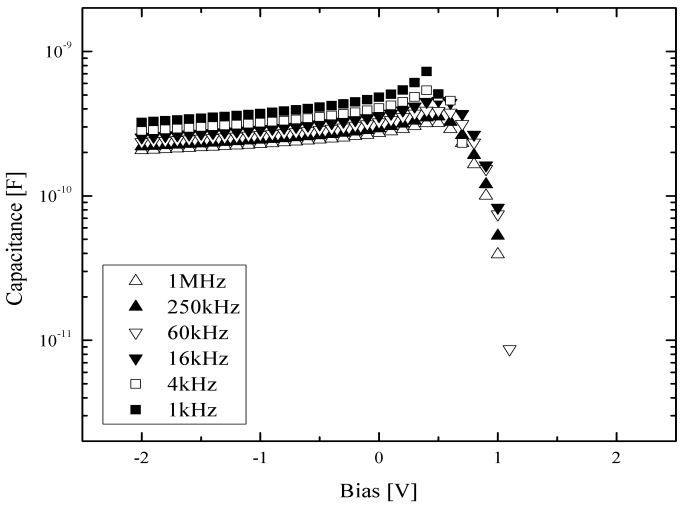

Figure B.6: The contact deposited on the O-face, unpolished Zn-face.

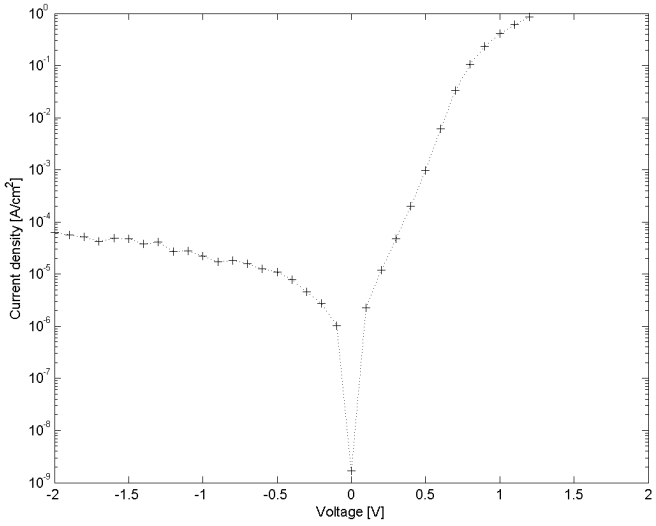

Figure B.7: The contact deposited on O-face, only O-face polished.

References

[1] C. W. Bunn. The lattice–dimensions of zinc oxide. *Proc. Phys. Soc. London*, 47:835, 1935.

[2] Victoria Anne Coleman. *Processing and characterization of ZnO for device applications **(and references therein)***. PhD thesis, The Australian National University, 2006.

[3] K. Ellmer, A. Klein, and B. Rech. *Transparent Conductive Zinc Oxide*. Springer, 2008.

[4] D. C. Look and B. Claflin. P-type doping and devices based on ZnO **(and references therein)**. *Physica Status Solidi B Basic Research*, 241:624–630, February 2004.

[5] SJ Pearton, DP Norton, K. Ip, YW Heo, and T. Steiner. Recent progress in processing and properties of ZnO. *Progress in Materials Science*, 50(3):293–340, 2005.

[6] N.H. Nickel and E. Terukov. *Zinc Oxide-a Material for Micro-and Optoelectronic Applications*. Kluwer Academic Pub, 2005.

[7] B. Claflin, DC Look, SJ Park, and G. Cantwell. Persistent n-type photoconductivity in p-type ZnO. *Journal of Crystal Growth*, 287(1):16–22, 2006.

[8] D.C. Look. Electrical and optical properties of p-type ZnO. *Semiconductor Science and Technology*, 20(4):S55–S61, 2005.

[9] Ben G. Streetman and Sanjay Banerjee. *Solid state electronic devices*. Prentice hall international, Inc., 5 edition, 2000.

[10] Charles Kittel. *Introduction to solid state physics*. Wiley, 8 edition, 2005.

[11] http://mrsec.wisc.edu/edetc/background/led/band.htm, 2008.

[12] Lars Sundnes Løvelie. Electrical characterization of majority carrier traps in electron irradiated epitaxial n-type Si. Master's thesis, University of Oslo, 2007.

[13] Stephen A. Campbell. *The science and engineering of microelectronic fabrication*. Oxford university press, 2 edition, 2001.

[14] Ü. Özgür, Y. I. Alivov, C. Liu, A. Teke, M. A. Reshchikov, S. Dogan, V. Avrutin, S. J. Cho, and H. Morkoç. A comprehensive review of ZnO materials and devices **(and references therein)**. *Journal of Applied Physics*, 98, August 2005.

[15] D. C. Look. Progress in ZnO materials and devices **(and references therein)**. *Journal of Electronic Materials*, 35:1299–1305, June 2006.

[16] R. E. Krebs. *The History and Use of Our Earth's Chemical Elements : A Reference Guide*. Greenwood Press, 2006.

[17] Gordon Aylward and Tristan Findlay. *SI Chemical Data*. John Wiley & Sons Australia, Ltd., 5 edition, 2002.

[18] M. G. Wardle, J. P. Goss, and P. R. Briddon. Theory of Li in ZnO: A limitation for Li-based p-type doping **(and references therein)**. *Physical Reviews*, 71(15), apr 2005.

[19] A. F. Kohan, G. Ceder, D. Morgan, and C. G. van de Walle. First-principles study of native point defects in ZnO. *Physical Review B: Condens. Matter Mater. Phys*, 61, 2000.

[20] F. Oba, S. R. Nishitani, S. Isotani, and I. Tanaka. First-principles study of native point defects in ZnO. *Journal of Applied Physics (824)*, 90, 2001.

[21] S. B. Zhang, S. H Wei, and A. Zunger. First-principles study of native point defects in ZnO. *Physical Review B: Condens. Matter Mater. Phys (075205)*, 63, 2001.

[22] C. G. van de Walle. Hydrogen as a Cause of Doping in Zinc Oxide **(and references therein)**. *Physical Review Letters*, 85:1012–1015, July 2000.

[23] S. Y. Myong, S J. Baik, C. H. Lee, W. Y. Cho, and K. S. Lim. Extremely transparent and conductive ZnO: Al thin films prepared by photo-assisted metalorganic chemical vapor deposition (photo-MOCVD) using AlCl3(6H2O) as new doping material. *Jpn. J. Appl. Phys.*, 36, 1997.

[24] H. von Wenckstern, R. Pickenhain, H. Schmidt, M. Brandt, G. Biehne, M. Lorenz, M. Grundmann, and G. Brauer. Deep acceptor states in ZnO single crystals. *Applied Physics Letters*, 89:092122, 2006.

[25] BK Meyer, J. Sann, DM Hofmann, C. Neumann, and A. Zeuner. Shallow donors and acceptors in ZnO. *Semicond Sci Technol*, 20:S62, 2005.

[26] D.M. Hofmann, A. Hofstaetter, F. Leiter, H. Zhou, F. Henecker, B.K. Meyer, S.B. Orlinskii, J. Schmidt, and P.G. Baranov. Hydrogen: A Relevant Shallow Donor in Zinc Oxide. *Physical Review Letters*, 88(4):45504, 2002.

[27] AR Hutson. Hall Effect Studies of Doped Zinc Oxide Single Crystals. *Physical Review*, 108(2):222–230, 1957.

[28] K. Minegishi, Y. Koiwai, Y. Kikuchi, K. Yano, M. Kasuga, and A. Shimizu. Growth of p-type Zinc Oxide Films by Chemical Vapor Deposition. *Jpn. J. Appl. Phys., Part*, 2:36, 1997.

[29] J. Fan and R. Freer. The roles played by Ag and Al dopants in controlling the electrical properties of ZnO varistors. *Journal of Applied Physics*, 77:4795, 1995.

[30] A.N. Gruzintsev, V.T. Volkov, and E.E. Yakimov. Photoelectric properties of ZnO films doped with Cu and Ag acceptor impurities. *Semiconductors*, 37(3):259–262, 2003.

[31] RE Dietz, H. Kamimura, MD Sturge, and A. Yariv. Electronic Structure of Copper Impurities in ZnO. *Physical Review*, 132(4):1559–1569, 1963.

[32] D. Pfisterer, J. Sann, DM Hofmann, M. Plana, A. Neumann, M. Lerch, and BK Meyer. Incorporation of nitrogen acceptors in ZnO powder. *Physica status solidi. B. Basic research*, 243(1):1–3, 2006.

[33] A. Onodera and N. Tamaki. Dielectric Activity and Ferroelectricity in Piezoelectric Semiconductor Li-Doped ZnO. *Jpn. J. Appl. Phys*, 35(9B Part 1):65160–65162, 1996.

[34] Goodwill. ZnO single crystal substrates. http://spcgoodwill.com/catalog_f.html, 2007.

[35] J. S. Christensen and B. G. Svensson. Secondary ion mass spectrometry. In manuscript.

[36] Jens S. Christensen. Secondary ion mass spectrometry. MEF3100 lecture slides, 2007.

[37] Ziyi Dai. Four Point Resistivity and Conductivity Type Measurements. http://www.mems.louisville.edu/lutz/resources/sops/sop45.html, 2007.

[38] ZYGO corporation. http://zygo.com/products/newview7000/nv7200spec.pdf, 2008.

[39] *White light interferometry – a production worthy technique for measuring surface roughness on semiconductor wafers*, Vancouver, British Columbia, Canada, apr 2006.

[40] B. G. Svensson, T. Moe Børseth, K. M. Johansen, T. Maqsood, R. Schifano, U. Grossner, J. S. Christensen, L. Vines, P. Kalson, Q. X. Zhao, M. Willander, F. Tuomisto, W. Skorupa, E. V. Monakhov, and A. Yu. Kuznetsov. Hydrothermally grown single-crystalline zinc oxide; characterization and modification **(and references therein)**. *Materials Research Society*, 2007.

[41] D. C. Look, B. Claflin, and H. E. Smith. Origin of conductive surface layer in annealed ZnO. *Applied Physics Letters*, 92(12), 2008.

[42] K. Jacobi, G. Zwicker, and A. Gutmann. Work function, electron affinity and band bending of zinc oxide surfaces. *Surface Science*, 141(1):109–125, 1984.

[43] MW Allen, P. Miller, RJ Reeves, and SM Durbin. Influence of spontaneous polarization on the electrical and optical properties of bulk, single crystal ZnO. *Applied Physics Letters*, 90:062104, 2007.

[44] K. Ip, M. E. Overberg, Y. W. Heo, D. P. Norton, S. J. Pearton, C. E. Stutz, S. O. Kucheyev, C. Jagadish, J. S. Williams, B. Luo, F. Ren, D. C. Look, and J. M. Zavada. Hydrogen incorporation, diffusivity and evolution in bulk ZnO. *Solid state electronics*, 2003.

[45] G. H. Kassier, M. Hayes, F. D. Auret, M. Mamor, and K. Bouziane. Electrical and structural characterization of as-grown and annealed hydrothermal bulk ZnO. *Journal of Applied Physics*, 102:4903–+, July 2007.

[46] E. H. Rhoderick and R. H. Williams. *Metal–semiconductor contacts*. Clarendon press, Oxford, 2 edition, 1988.

[47] P. Blood and J. W. Orton. *The electrical characterization of semiconductors: majority carriers and density states*. Academic press, 1992.

[48] O. Schmidt, P. Kiesel, van de Walle, N. M. Johnson, J. Nause, and G. H. Döhler. Effects of an electrically conducting layer at the zinc oxide surface. *Jpn. Journal of Applied Physics*, 44:7271, 2005.

[49] H. K. Kim, S. H. Han, T. Y. Seong, and W. K. Choi. Low–resistance ti/au ohmic contacts to al–doped ZnO layers. *Applied Physics Letters*, 77:1647, September 2000.

[50] Israel Vagner. http://www.hit.ac.il/staff/vagner/Schottky.PDF, 2008.

[51] R. Schifano, E. V. Monakhov, U. Grossner, and B. G. Svensson. Electrical characteristics of palladium Schottky contacts to hydrogen peroxide treated hydrothermally grown ZnO. *Applied Physics Letters*, 91:3507–+, November 2007.

[52] U. Grossner, S. Gabrielsen, T. B. Børseth, J. Grillenberger, A. Yu. Kuznetsov, and B. G. Svensson. Palladium Schottky barrier contacts to hydrothermally grown n-ZnO and shallow electron states. *Applied Physics Letters*, 85, September 2004.

[53] K. Ip, B. P. Gila, A. H. Onstine, E. S. Lambers, Y. W. Heo, K. H. Baik, D. P. Norton, S. J. Pearton, S. Kim, J. R LaRoche, and F. Ren. Improved Pt/Au and W/Pt/Au Schottky contacts on n-type ZnO using ozone cleaning. *Applied Physics Letters*, 84(25):5133–5135, 2004.

[54] H. von Wenckstern, E. M. Kaidashev, M. Lorenz, H. Hochmuth, G. Biehne, J. Lenzner, V. Gottschalch, R. Pickenhain, and M. Grundmann. Lateral homogeneity of Schottky contacts on n-type ZnO. *Applied Physics Letters*, 84(1):79–81, 2004.

[55] Sang-Ho Kim, Han-Ki Kim, and Tae-Yeon Seong. Electrical characteristics of Pt Schottky contacts on sulfide-treated n-type ZnO. *Applied Physics Letters*, 86(2):022101, 2005.

[56] H.S. Kang, S.S. Pang, J.W. Kim, G.H. Kim, J.H. Kim, S.Y. Lee, Y. Li, H. Wang, and QX Jia. The role of a ZnO buffer layer in the growth of ZnO thin film on Al2O3 substrate. *Superlattices and Microstructures*, 40(4-6):501–506, 2006.

[57] Q. L. Gu, C. C. Ling, X. D. Chen, C. K. Cheng, A. M. C. Ng, C. D. Beling, S. Fung, A. B. Djurišić, L. W. Lu, G. Brauer, and H. C. Ong. Hydrogen peroxide treatment induced rectifying behavior of Au/n-ZnO contact. *Applied Physics Letters*, 90(12), 2007.